Amphiphilic Model Networks Based on PEG and PCL Tetra-Arm Star Polymers with Complementary Reactivity

Carolin Bunk,[1,2] Lucas Löser,[3] Nora Fribiczer,[4] Hartmut Komber,[1] Lothar Jakisch,[1] Reinhard Scholz,[1] Brigitte Voit,[1,2] Sebastian Seiffert,[4] Kay Saalwächter,[3] Michael Lang,[1*] Frank Böhme[1]**

[1] Leibniz-Institut für Polymerforschung Dresden e. V, Hohe Str. 6, 01069 Dresden, Germany

[2] Organic Chemistry of Polymers, Technische Universität Dresden, 01062 Dresden, Germany

[3] Institut für Physik - NMR, Martin-Luther-Universität Halle-Wittenberg, Betty-Heimann-Str. 7, 06120 Halle, Germany

[4] Department of Chemistry, Johannes Gutenberg University Mainz, Duesbergweg 10-14, 55128 Mainz, Germany

KEYWORDS Amphiphilic co-networks, hetero-complementary coupling reactions, model networks, multiple quantum NMR, swelling, rheology, viscometry, interaction parameter

TOC graphic for Table of Contents use only.

ABSTRACT

A new approach for the synthesis of model amphiphilic polymer co-networks (ACN) based on a hetero-complementary reaction of a 2-(4-nitrophenyl)-benzoxazinone terminated tetra-arm polycaprolactone star (tetra-PCL) with an amino-terminated tetra-arm polyethylene glycol star (tetra-PEG) is presented. The reaction conditions (solvent, concentration, temperature) were varied widely. Reaction kinetics and gelation were analyzed with high resolution NMR spectroscopy and computer simulations. The results agree with a nearly homogeneous mixture where local composition fluctuations affect kinetics only after most of the molecules are attached to the gel. Viscometry, dynamic light scattering data and literature data for the solubility parameters were combined to provide estimates for the Flory-Huggins interaction parameter of the two star polymers in toluene, chloroform, and THF as solvents. These estimates allow to collapse equilibrium swelling data in different solvents on a universal curve. Multiple quantum NMR analysis shows an enhanced formation of double connections between the same pair of stars as compared to preceding work on tetra-PEG gels made by the same cross-linking strategy but with a different coupling reaction. Besides of this last observation, the remaining results indicate that the networks possess a near model like structure with only a small fraction of pending arms as most relevant type of network defects.

INTRODUCTION

Model amphiphilic polymer co-networks (ACNs) are tailor-made adaptive soft solids of covalently crosslinked polymers with both hydrophilic and hydrophobic units.[1-6] Based on their amphiphilicity, ACNs swell independently in water as well as in organic solvents.[7-9] The resulting environmentally-sensitive viscoelasticity and selective permeability make them suitable for deliberately controlling the transport of molecules of different polarity through the swollen polymer network (gel).[6] The latter is exploited for soft contact lenses with extended wear time, the most common application of ACNs.[10-12] Further, biomedical applications are (multi) stimuli-responsive functionalized ACN-based matrices or membranes especially for drug delivery devices[13-18], but also for tissue engineering[19] and bioartificial pancreas.[20] In addition, potential technological uses of ACNs are being explored as biocatalyst supports,[21] sensors,[22, 23] and polymer electrolytes for batteries.[24] The properties for all these and other applications are controlled by the polymer network structure, which in turn is strongly dependent on the formation process. A very good overview on the synthesis of ACNs is provided in the review by Erdodi and Kennedy.[6] A major concern of some authors cited there was to obtain networks with defined structure. Although very promising results were achieved in some cases, the attained structures did not comply the criteria of a model network, which is characterized by a homogenous structure of defined length and number of monodisperse polymer strands connected together by junction points of known and constant functionality within an infinite three-dimensional net structure.[4, 25]

A seminal paper published by Sakai *et al.*[26] in 2008 showed one possible way to obtain hydrophilic star-polymer networks with model network structure. Their approach is based on an end-linking process through a hetero-complementary conversion of two four-arm polyethylene glycol stars (A_4- and B_4-type tetra-PEG) containing different reactive end groups. For star

polymers with narrow polydispersity, the number of chain segments between the network junctions is well-fined. Furthermore, the hetero-complementary conversion of the terminal groups avoids that arms of one star react with each other. This eliminates the formation of a significant part of undesirable microscopic defects,[27] leading to a substantial enhancement of the elastic modulus of the networks when prepared at a low overlap number of the network strands.[28] Gels synthesized in this way are characterized by excellent mechanical stability and homogeneity.[29-31] The structure of such gels is quite close to that of a model network, but still structural defects, like pending arms and double or multiple links between the star polymers develop due to the statistical nature of the cross-linking process.[32] In particular, double links with adjacent stars (see **Scheme 1**) can be detected and quantified by low-field ^{1}H multiple-quantum nuclear magnetic resonance (MQ NMR) spectroscopy[33] and Monte-Carlo simulations,[32] which provides detailed insight into the topology of the networks. In recent years, synthesis and characterization of networks with well-defined structures have raised the understanding of their structure-property relations to a new level. In contrast, corresponding studies on amphiphilic co-networks have been performed only sporadically to date.[8, 9, 34, 35] With our contribution, we aim to advance the state of knowledge regarding structure-property relationships of model amphiphilic co-networks.

In analogy to the tetra-PEG gels, a key aspect in the synthesis of model ACNs is the hetero-complementary linkage of structurally defined hydrophilic and hydrophobic star polymers via their end groups. Typically, fast click reactions, such as azide-alkyne cycloaddition,[36] condensation reactions of amino groups with activated ester bonds,[9, 34] as well as the addition reaction of benzaldehyde and benzaacylhydrazide terminal groups[8] have been used for the synthesis of A_2B_4- and A_4B_4-type ACNs. These reactions provide high conversions within a short time. While this may initially appear to be an advantage, it entails the risk that the components forming the network

do not mix properly. As a result, additional defects and large-scale heterogeneities inducing shielding of reactive groups may occur. Another influencing factor is a possible segregation of the chemically different building blocks during the ACN formation, which is also assumed to have an effect on network inhomogeneities. These aspects have hardly been considered in previous work. To address this challenge of minimizing structural network defects, a homogeneous reaction mixture prior to gelation is essential, especially for systems based on components of different polarity. Accordingly, in addition to a hetero-complementary end group reaction with high conversion, a sufficiently slow and adjustable viscosity increase is of particular importance, i.e., a cross-linking reaction with an adjustable moderate reaction rate and a suitable non-selective solvent for both star polymers is desired.

In previous work, we used 2-phenylbenzoxazinone-based compounds to functionalize polymers with oxazinone groups.[37, 38] By reaction of these oxazinone-functionalized polymers with amino group containing polymers, block and graft copolymers were obtained. As a proof of concept, we also synthesized A_2-B_4 hybrid networks by conversion of an oxazinone-terminated 4-arm poly-ε-caprolactone star with a linear amino-terminated polypropylene glycol prepolymer.[39] A major advantage of the oxazinone-amine reaction is their controllable reactivity. By introducing electron withdrawing substituents on the oxazinone group and varying the reaction temperature, the course of the reaction can be significantly influenced, offering great potential for the synthesis of well-defined ACNs.

Focusing on material properties and application, but without addressing the network formation process and its influence on network defects, synthesis of highly biocompatible and biodegradable ACNs based on hydrophobic PCL and hydrophilic PEG have been reported several times in the literature.[40-42] ACNs with these components are also subject of the present publication, but, with

special focus on the process of network formation. With the aim of obtaining networks with highly defined structures, the synthesis was carried out following the tetra-arm approach of Sakai *et al.*[26] In contrast to Sakai, in our method presented here, hydrophobic PCL and hydrophilic PEG tetra-arm stars were linked by the much slower 2-(4-nitrophenyl)-benzoxazinone/amine reaction in organic solvents similar as described earlier for the synthesis of A_2-B_4 hybrid networks.[39] In our approach, hydroxy-terminated star polymer tetra-PCL (**1**) was first reacted with 2-(4-nitrophenyl)-4-oxo-4H-benzo[d][1,3]oxazine-7-carboxylic acid chloride (**2**), resulting in 2-(4-nitrophenyl)-benzoxazinone-terminated tetra-PCL (**3**), which was cross-linked in different organic solvents with amino-terminated star polymer tetra-PEG (**5**) in a second step to give ACN gels (see **Scheme 1**). The moderate rate of the cross-linking reaction allows the precursor star polymers to mix and diffuse and, moreover, to monitor this process by NMR spectroscopy and oscillatory shear rheology.

Our main concern is to show how the reaction conditions influence the course of the reaction and thus the microstructure and homogeneity of ACNs. In particular, we study the influence of the reaction conditions (solvent, concentration and temperature) on the cross-linking process and the occurrence of associated network defects. The solvent quality of toluene, tetrahydrofuran, and chloroform as possible non-selective solvent is analyzed by using a combined approach of viscosity measurements and theoretical computations. Furthermore, the resulting environment-dependent viscoelasticity and swelling behavior of the gels prepared under different reaction conditions are investigated. We have also used large-scale computer simulations to model network formation under idealized conditions (perfect stars, all reactive groups reactive, perfect mixing of both components). Comparison with these data allows to explore deviations from ideal reaction conditions and possible de-mixing effects.

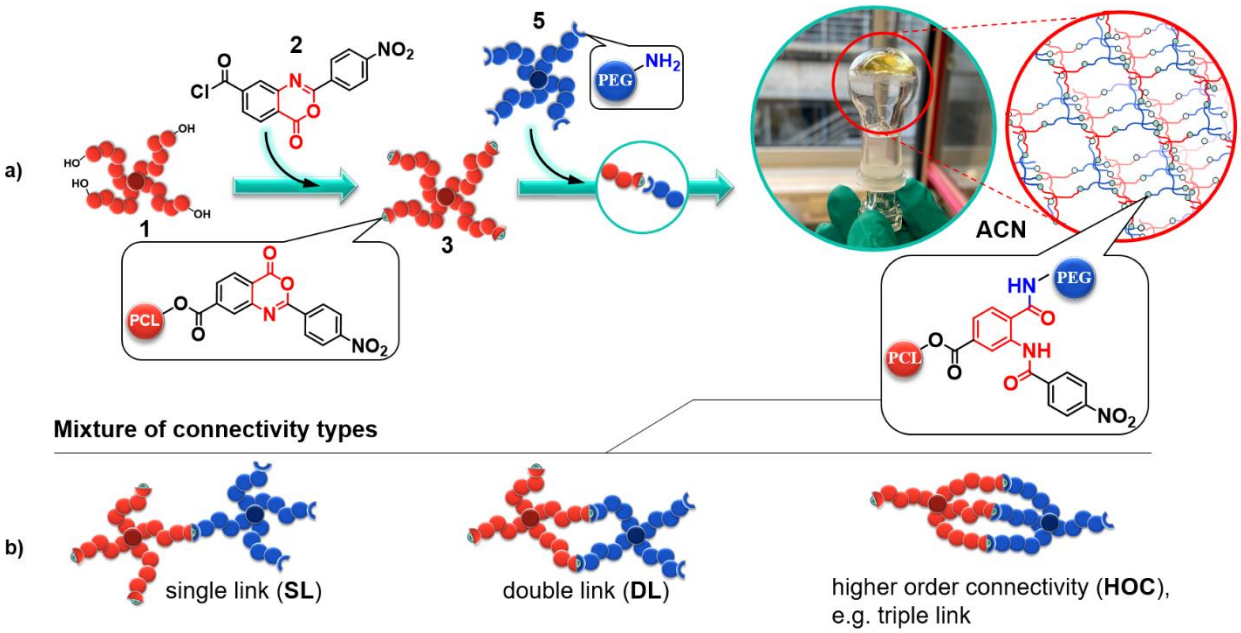

Scheme 1. Synthesis of ACNs based on hydrophobic 2-(4-nitrophenyl)-benzoxazinone-terminated PCL (**3**) and hydrophilic amino-terminated PEG (**5**) tetra-arm star polymers, a) reaction scheme, b) connectivity types within the polymer network formed.

EXPERIMENTAL SECTION

Materials

All chemicals and solvents (analytical grade) were obtained from Sigma-Aldrich and used as received unless differently mentioned. Hydroxy-terminated tetra-arm polyethylene glycol (tetra-PEG-OH) was obtained from JenKem Technology USA and purified by dialysis in water (ZelluTrans, Roth, 1000 g mol^{-1} molecular weight cutoff) and precipitated twice from THF in cold diethyl ether. The number-average molar mass (M_n) was determine by SEC-MALLS in water (M_n = 10 kg mol^{-1}, Đ = 1.02). ε-Caprolactone (ε-CL) was dried under reduced pressure over CaH_2 for at least 24 hours, then purified by vacuum distillation and stored under nitrogen atmosphere. Tin(II)-2-ethylhexanoate ($Sn(oct)_2$) was purified by vacuum distillation and stored under nitrogen atmosphere. 2-(4-Nitrophenyl)-4-oxo-4H-benzo[d][1,3]oxazine-7-carboxylic acid chloride (**2**) was synthesized as described earlier.[39]

Synthesis of functionalized tetra-arm star polymers

*2-(4-Nitrophenyl)-benzoxazinone-terminated tetra-PCL (**3**)*

Star polymer **3** was synthesized according to **Scheme 2a** in two steps as previously reported.[39, 43] At first, **1** was synthesized by ROMP of ε-CL using pentaerythritol as starter and $Sn(oct)_2$ as catalyst. The molar ratio of ε-CL : pentaerythriol : $Sn(oct)_2$ was adjusted to 87 : 1 : 0.1. Subsequently, the hydroxy terminal groups of **1** were converted with compound **2** to yield **3**.

^{1}H NMR (THF-d_8, 40°C): δ 8.53 (d, 8.9 Hz; 10), 8.39 (d, 8.9 Hz; 11), 8.32 (d, 1.5 Hz; 7), 8.29 (d, 8.1 Hz; 8), 8.18 (dd, 8.1 Hz, 1.5 Hz; 9), 4.39 (t, 6.6 Hz; 6 next to OC(O)Ph), 4.12 (s; 1), 4.02 (t, 6.7 Hz; 6), 2.32 (t, 7.4 Hz; 4 next to core), 2.26 (t, 7.4 Hz; 2), 1.65 – 1.55 (3, 5), 1.38 ppm (m; 4), see also SI **Figure S1** and **S3c**. The complete ^{1}H and ^{13}C NMR characterisation data (solvent: $CDCl_3$) of **3** are reported in an earlier publication.[43]

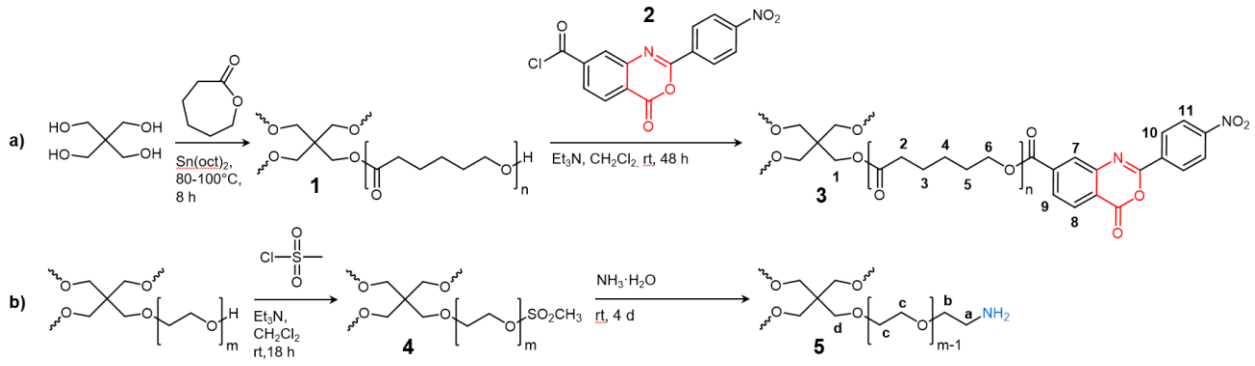

Scheme 2. Synthesis of tetra-arm star polymers **3** and **5**.

Mesylate-terminated tetra-PEG (4)

Star polymer **4** was synthesized by adapting a previously reported procedure (see first step in **Scheme 2b**).[44] Briefly, purified tetra-PEG-OH (10 g, 1 mmol) with a number-average molar mass of 10 kg mol^{-1} was dissolved in 50 mL anhydrous CH_2Cl_2 under nitrogen atmosphere. Then 8.5 mmol of triethylamine and 8 mmol of mesylchloride were added to the solution and stirred overnight. After the reaction, the mixture was filtered to remove insoluble triethylamine hydrochloride, concentrated in vacuo and poured into a 10-fold excess of cold diethyl ether. The precipitated star polymer **4** (9.1 g, 91%) was isolated by filtration and dried in vacuo at 40 °C.

^{1}H NMR ($CDCl_3$): δ 4.37 (t, 8H; SO_2OCH_2), 3.76 (m, 8H; $SO_2OCH_2CH_2$), 3.70–3.45 (CH_2CH_2), 3.41 (s; $CH_{2,core}$), 3.07 ppm (s, 12H; CH_3SO_2).

Amino-terminated tetra-PEG (5)

Star polymer **5** was prepared as described earlier (see second step in **Scheme 2b**).[44] Briefly, star polymer **4** (9 g, 0.9 mmol) was dissolved in 28 % aqueous ammonia solution (100 mL). The reaction mixture was left with stirring for 4 days at room temperature. The ammonia was allowed to evaporate over night after NaOH (5 M) was added dropwise until the pH reached 13. The solution was dialyzed several times against deionized water for 24 h. The aqueous solution was

concentrated in vacuo and the water was completely removed by lyophilization to give **5** (7.2 g, 80%).

^{1}H NMR (THF-d_8, 40°C): δ 3.55 (s; c), 3.42 (br; b), 3.41 (s; d), 2.76 (br; a), 2.36 ppm (v br; NH_2 and water from solvent), see also SI **Figure S2**.

Synthesis of amphiphilic co-networks (*CN*)

A series of amphiphilic co-networks **CN** was synthesized by hetero-complementary reaction of the end groups of **3** and **5**.

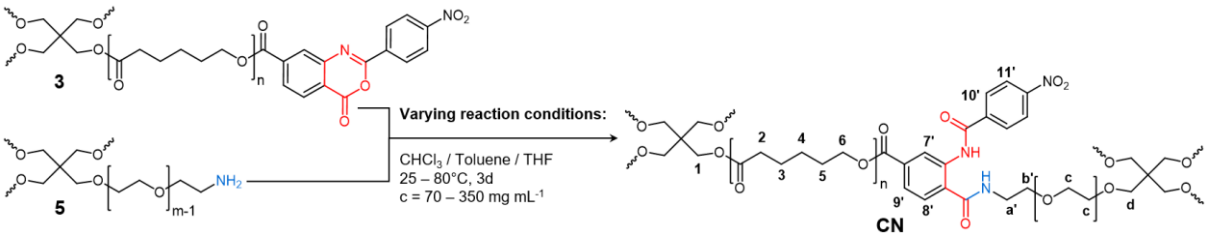

Scheme 3. Synthesis of amphiphilic co-networks (**CN**).

For the synthesis, the polymer concentration, the temperature and the solvents were varied. A sample overview is given in **Table 1**.

First, stock solutions of **3** and **5** with different polymer volume factions (ϕ = 0.06, 0.18, 0.30) were prepared. The ϕ values correspond roughly to 1, 3, and 5 times the overlap concentration c* (70 mg mL^{-1}), which appears as last part of the sample name (e.g. **CN1-1**, **CN1-3**, **CN1-5** are synthesized at 1c*, 3c*, 5c*, respectively). For the synthesis, aliquots of the stock solutions were poured together at a certain temperature and allowed to react. After reaching the gel point (visual detection), the temperature was raised to the final reaction temperature until cross-linking was completed. To ensure equivalence of the reactive groups, ^{1}H NMR spectra of mixtures of the stock solutions were recorded. Based on the intensities of the end group signals, concentration

differences of the reactive groups could be compensated by post-dosing of the deficiency component.

The synthesis of **CN2-1** in THF (ϕ = 0.06) is described in the following as an example: To start the cross-linking, 0.972 g of the stock solution of **5** was placed in a 5 mL reaction flask equipped with a flat stirrer using a 1 mL syringe. Then, 0.784 g of the stock solution of **3** was added, and the reaction flask was tightly closed. The reaction mixture was stirred at 25 °C until gelation was observed. After this, the reaction flask was placed in a preheated oil bath (40 °C) for three days.

^{1}H NMR (THF-d_8, 40°C): δ 12.94 (br; PhN*H*CO), 9.49 (d, 1.3 Hz; 7'), 8.38 (d, 8.5 Hz; 10'), 8.33 (t; CH_2N*H*CO), 8.25 (d, 8.5 Hz; 11'), 8.88 (d, 8.3 Hz; 8'), 7.77 (dd, 8.3 Hz, 1.3 Hz; 9'), 4.34 (t, 6.5 Hz; 6 next to OC(O)Ph), 4.12 (s; 1), 4.02 (t, 6.7 Hz; 6), 3.67 (t; a'), 3.55 (b', c), 3.42 (s; d), 2.32 (t, 7.4 Hz; 4 next to core), 2.26 (t, 7.4 Hz; 2), 1.65 – 1.55 (3, 5), 1.38 ppm (m; 4). The data are related to the kinetics experiments and were determined from a low-conversion sample. The signals are significantly broadened at higher conversion and for the final networks (see SI **Figure S3a,b**). The assignments are in accordance with data reported in our recent study on soluble tetra-arm polymers containing the same structural motif.[43] A part of the analysis (rheology, NMR) requires a modified preparation that is explained in the corresponding sections below.

For comparison, PEG-PEG networks were synthesized by the Sakai active-ester linking chemistry in water[26] (**PEG-1**) and by conversion of **5** with oxazinone-terminated tetra-PEG in toluene (**PEG-2**). In each case, tetra-PEG-OH (M_n = 10 kg mol^{-1}) was used as starting material for the syntheses.

Table 1 Sample Overview

Sample	Solvent	ϕ_0 [a]	T_1 [b] (°C)	T_2 [c] (°C)	p [d]	Q_v [e]				w_{sol} [f] (%)	f_{defs} [g]
						1	2	3	4		
CN1-1	THF	0.06	25	25	0.98	20.9	13.2	10.4	10.2	8	-
CN2-1	THF	0.06	25	40	0.99	20.0	14.0	10.7	10.2	9	-
CN3-1	THF	0.06	25	60	0.99	19.6	15.2	11.6	10.2	9	-
CN1-3	THF	0.18	25	25	0.98	11.7	10.2	9.4	9.0	2	-
CN2-3	THF	0.18	25	40	0.99	11.4	10.7	9.5	8.8	4	-
CN3-3	THF	0.18	25	60	0.99	11.6	10.7	9.3	9.3	2	-
CN2-5	THF	0.30	25	40	0.84	9.2	8.7	8.2	7.8	1	-
CN3-5	THF	0.30	25	60	0.99	8.2	7.9	8.1	7.7	1	-
CN4-1	THF-d_8	0.06	40	80	-	20.0	14.0	13.6	-	-	9
CN5-1	THF-d_8	0.06	60	60	-	20.5	14.1	13.5	-	-	5
CN4-3	THF-d_8	0.18	40	80	-	15.1	13.6	13.6	-	-	2
CN5-3	THF-d_8	0.18	60	60	-	14.8	13.4	13.6	-	-	1
CN6-1	toluene-d_8	0.06	40	80	-	19.4	12.2	12.0	-	-	3
CN7-1	toluene-d_8	0.06	60	60	-	17.1	11.8	11.5	-	-	3
CN6-3	toluene-d_8	0.18	40	80	-	11.0	10.4	9.8	-	-	1
CN7-3	toluene-d_8	0.18	60	60	-	11.1	10.0	10.4	-	-	1
CN8-1	$CDCl_3$	0.06	40	80	-	28.5	22.1	20.6	-	-	28
CN9-1	$CDCl_3$	0.06	60	60	-	30.9	23.3	22.7	-	-	-
CN8-3	$CDCl_3$	0.18	40	80	-	23.6	21.9	21.3	-	-	0
CN9-3	$CDCl_3$	0.18	60	60	-	23.2	21.8	22.2	-	-	0
PEG-1[h]	D_2O	0.15	25	25	-	32.3	-	-	-	-	10
PEG-2	toluene-d_8	0.15	25	25	-	10.8	-	-	-	-	1

[a] polymer volume fraction at preparation

[b] reaction temperature before reaching the gel point

[c] reaction temperature after reaching the gel point

[d] degree of conversion determined by ^{1}H HR MAS NMR spectroscopy after removal of the sol fraction, evaporation of the reaction solvent, and reswelling in D_2O

[e] gravimetrically determined equilibrium volume swelling degree (columns 1-4 refer to four consecutive measurements with intermediate drying steps)

[f] sol fractions gravimetrically determined for **CN1** to **CN3**

[g] defect fractions determined by MQ NMR spectroscopy

[h] synthesized according to Sakai *et al.*[26]

Characterization

Size Exclusion Chromatography (SEC). The number-average and weight-average molar masses (M_n and M_w) and the molar mass distribution (Đ) of the tetra-PCL-based star polymers **3a-c**, **5b** and **5c** presented in **Table 2** were determined using an isocratic HPLC pump (Agilent 1200) with autosampler (Agilent Technologies, Santa Clara, CA) equipped with twofold detection (SEC-MALS/dRI). Details are described in the SI **Chapter 5**.

Viscometry. Overlap concentrations c* of star polymers **3** and **5** in THF, toluene and chloroform were determined by capillary viscometry using equation (1), adopting the same convention as for linear polymers,[45]

$$[\eta] = \lim_{c \to 0} \frac{\eta_{sp}}{c} = \frac{1}{c^*} \quad (1)$$

where η_{sp} is the specific viscosity and $[\eta]$ the intrinsic viscosity of the solutions. Measurements were performed at 25 and 35 °C. The evaluation was carried out according to Schulz-Blaschke.[46] Details are described in the SI **Chapter 6** (**Table S1**).

Dynamic Light Scattering (DLS). The hydrodynamic radii R_h of compounds **3** and **5** in THF were determined by DLS measurements using the Stokes-Einstein equation

$$R_h = \frac{k_B T}{6\pi\eta_s D} \quad (2)$$

where k_B is the Boltzmann constant, T the absolute temperature, η_s the viscosity of the solvent, and D the diffusion coefficient. The measurements were performed on a light scattering setup equipped with an ALV-SP125 goniometer, an ALV/LSE5004 multi tau correlator, a fiber optical ALV/High QE APD avalanche photodiode with pseudo-cross correlation and a uniphase He/Ne laser (632.8 nm, Thorlabs Inc.). Details of the DLS analysis are described in the SI **Chapter 7**. Results are presented in **Tables S2** and **S3** of the SI.

Equilibrium swelling experiments. Equilibrium volume swelling degrees Q_v were determined at room temperature. As-prepared co-networks (gel) were first placed in a large amount of the synthesis solvent for 48 hours to remove the sol fraction.

Subsequently, the gels where separated from the swelling medium and weighted. After drying in a vacuum oven at 40 °C, the weight of the polymer (w_p) was determined while the solvent weight in the swollen gel (w_s) is the weight loss of the sample during drying. Q_v was determined as follows

$$Q_v = 1 + \left(\frac{\rho_p}{\rho_s}\right)\left(\frac{w_s}{w_p}\right). \quad (3)$$

Here, ρ_s is the density of the used swelling solvent and ρ_p is the density of the polymers (1.13 g mL^{-1} as average for both PEG and PCL).[47] The procedure of swelling the samples to equilibrium followed by complete drying was repeated up to three times for all networks. As a result, equilibrium degrees of swelling (Q_{v1}, Q_{v2} etc.) were measured, where the index counts the number of the swelling experiment.

Rheology. Rheological measurements were performed on an Anton Paar modular compact rheometer of type MCR 302 (Anton Paar, Graz, Austria) equipped with a plate-plate geometry of type PP25 with a plate diameter of 25 mm. A Peltier plate was used to control the temperature and a solvent trap was used to prevent evaporation of the solvent. Gels were prepared from

homogenized equimolar mixtures of stock solutions of **3** and **5** in a mold fitting exactly the dimension of the probe geometry. The mixture was allowed to react overnight at room temperature. Frequency sweeps were carried out at a shear deformation of $\gamma = 1\%$ and in the range of $\omega = 1$ - 100 rad·s^{-1}. Storage moduli averaged over the full frequency range are shown in the SI **Chapter 8** (**Table S4**).

High resolution solution NMR spectroscopy. ^{1}H NMR spectra (500.13 MHz) were recorded on an Avance III 500 spectrometer (Bruker Biospin). $CDCl_3$ ($\delta(^1H) = 7.26$ ppm) and THF-d_8 ($\delta(^1H) = 1.72$ ppm) were used as solvent, lock, and internal standard. Sample temperature was kept constant (30 ± 0.5 °C), unless otherwise specified, using a BVT-3000 unit.

The reaction kinetics of the co-network formation was followed by *in situ* ^{1}H NMR spectroscopy in THF-d_8 at $\phi = 0.06$ and T= 25, 40, and 60 °C, respectively. For the measurements, stock solutions of **3** and **5** were prepared and combined with an equimolar ratio of reactive groups in a 5 mm NMR tube using a glass syringe and a precision balance. The tube was then sealed with a rubber septum, shaken sufficiently and immediately placed in the pre-heated NMR probe. After reaching the reaction temperature within approximately 5 min, the measurements were started. Sixteen scans with an acquisition time of 1.93 s and a delay time of 10 s were collected, resulting in a total experiment time of 191 s for each measurement. The normalized intensities of the signals at 9.5 ppm ($H_{7'}$ of **CN**) and 8.53 ppm (H_{10} of **3**) were used to calculate the conversion $p = I(H_{7'})/[I(H_{7'}) + 0.5 * I(H_{10})]$ of the cross-linking reaction. Inversion-recovery T_1 measurements on **3** and on a **CN** in THF-d_8 at 40 °C give T_1 values of 3.0 s for H_{10} and 3.4 s for $H_{7'}$. Thus, with an interval between the 90° ^{1}H pulses of ~12 s, an equal and almost complete T_1 relaxation (97% vs. 98%) of both protons occurs. Errors result mainly from the signal overlaps that occur at higher conversions, since the network formation leads to significant line broadening.

High resolution (HR) MAS NMR spectroscopy. The measurements were performed on an Avance III 500 NMR spectrometer with a Bruker HR MAS probe using a ZrO_2 rotor (4 mm outer diameter) with a PTFE insert (50 µL insert volume). For the measurements, the insert was filled with the dried co-networks (~2 mg). After addition of $CDCl_3$ (~50 µL) and a swelling time of 30 minutes, the spectra were recorded at 30 °C with a rotation frequency (ν_r) of 4650 Hz. Under these conditions, minimal overlap of signals and spinning sidebands was observed. The conversion was determined from the integral intensities of a signal of the reacted benzoxazinone group ($H_{7'}$ of **CN**; 9.5 ppm) and of the non-reacted benzoxazinone group (H_{10} of **3**; 8.53 ppm) as described for the kinetics experiments.

MQ NMR spectroscopy. Static proton solid-state NMR experiments for the quantification of connectivities and isotropic fraction are based upon the existence of motion-averaged residual dipolar couplings (RDCs) among the protons, which are non-zero for network chains that are fixed at their ends. At low overlap of the network strands (the entanglement-free limit), the magnitudes of the measured RDCs reflect roughly the elastic contribution of the respective chains and their connectivities (see **Scheme 1**).[48,49] Experiments were carried out on a Bruker mq20 MiniSpec with the specifications mentioned in the SI. The experiment provides two signal functions as a function of a double-quantum pulse sequence duration (DQ evolution time τ_{DQ}): the DQ intensity build-up (I_{DQ}) reflecting the magnitude of the RDCs and a reference intensity (I_{ref}). The sum of these two signals, referred to as summed multiple-quantum intensity ($I_{MQ} = I_{DQ} + I_{ref}$) corresponds to a full dipolar echo and is used to quantify and thus compensate for transverse relaxation effects (long-time signal loss). These data were evaluated similar to Lange *et al.* [33], except for some relevant procedural differences that will be explained below. Comparable data analysis was also applied on other tetra-arm star polymer systems.[50,51] Typically, three types of connectivities can be

distinguished differing sufficiently in their RDC as shown in **Scheme 1** (SL, DL, HOCs). This 3-component fit was assumed to be a proper modelling choice for our system, since the chemical and steric differences between PEG and PCL chains are small (see SI **Table S3)** and because all elastic strands contain a PCL and a PEG block that are under the same tension. Both types of macromonomers are dominated by trains of CH_2 groups, justifying the assumption that the measured RDCs of the different macromonomers are similar. Therefore, we will stick to the model of the three Abragam-like (A.-l.) functions representing one connectivity fraction each, as proposed in Ref.[52]

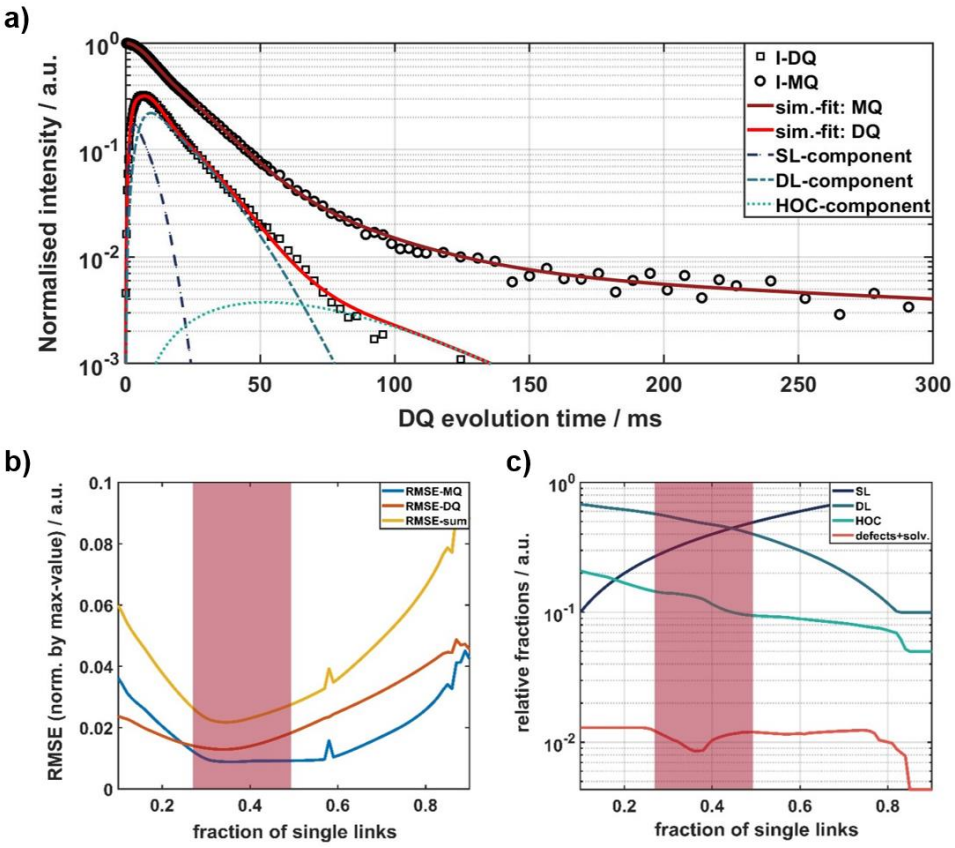

Figure 1 a) Exemplary fit of MQ NMR data of sample **CN6-3**, b) RMSE minimum, c) dependence of relative connectivity fractions corresponding to the respective fixed SL fraction value.

Further, the equality of the RDCs of PEG and PCL subchains was qualitatively confirmed in preliminary chemical shift resolved RDC measurements using the POST-C7 sequence[53]. Details will be reported elsewhere. As shown exemplarily in **Figure 1a**, the proposed 3-component fit well reproduces all features in both signals.

In contrast to Lange *et al.*,[33] we refrain from a global optimisation algorithm and instead propose another simultaneous fitting procedure of I_{MQ} and I_{DQ} data. We decided to minimise the summed normalised root-mean-squared error (nRMSE) of both functions using a self-written MatLab 2018b script, where the total RMSE was minimised using the MatLab fmincon algorithm for constrained, non-linear optimisation procedures. We follow a grid-search based procedure that replaces the global optimisation procedure by Lange *et al.* [33]:

The most relevant parameter, being the fraction of single links f_{SL}, is fixed, and the fit is carried-out with one fixed parameter, automatically stabilising the whole procedure. Afterwards, the f_{SL}-parameter is incremented by a small step Δf_{SL} (here $\Delta f_{SL} = 0.01 = 1\%$), and the fit evaluated again. This is done over the whole range of expected a1-values (here: between 0.1 and 0.9). The total RMSE is plotted (see **Figure 1b** and **1c**), and the minimum is detected and is taken as the best-fit result. The stability of the fit was tested by using randomly determined starting parameters within a physically meaningful range. The presented error bars (confidence boundaries) were chosen such that the corresponding curves present suitable envelopes for the data up to a 30 % increase of the nRMSE minimum value. Since the minimum is taken as reference value, error bars for the presented data are not symmetric and represent the range of possible values. We stress that the error bars describe a possible *systematic* error (possible fitting bias, e. g. arising from the fact that a single A.-l. function may not be a perfect approximation to a signal fraction), which means that trends in the best-fit results for different samples are meaningful even if they are smaller than this

systematic variation range. Other sources of errors, e.g., rf-pulse miscalibration or ambiguities in the distinction of different connectivities are not (or in the latter case only partially) included into the error bars. The fitting ambiguity between DL and HOC is circumvented by evaluating mostly the better defined single-link fraction and comparing it to the sum of other connectivities. Connectivity distributions of ACNs investigated are summarized in the SI **Chapter 9** (**Table S5**).

Computer simulations. Stoichiometric solutions of two different tetra-arm star polymers were equilibrated using a GPU-Version[54, 55] of the Bond-Fluctuation model.[56] The number of Kuhn segments per star arm in the simulations[57] was chosen to be roughly comparable with the experiments based upon literature data for the properties of Kuhn segments of PEG and PCL (see SI **Table S3**).[58, 59] After equilibration of the sample, reactivity of the end groups was turned on and reactions were possible only upon collision of two different reactive groups mimicking the hetero-complementary coupling of the stars in the experiments, see Ref.[32] for more details. Reaction kinetics was followed for 10 independent samples at five different concentrations between approximately 1 and 4 times the overlap concentration of the star polymers (for more details see SI **Chapter 12**). Gelation was detected by analyzing molecular weight distributions as described recently.[60] In a subsequent simulation, a series of gels prepared at a broader range of concentrations were swollen to equilibrium, and the equilibrium degree of swelling was determined from the average polymer volume fraction inside the swollen gel. More details on the simulations with a particular focus on equilibrium swelling properties and the residual bond orientations are available in Ref.[61]

RESULTS AND DISCUSSION

Synthesis and characterization of tetra-arm star polymers 3 and 5, and analysis of their interactions with solvents

The hydrophobic tetra-PCL-based **3** was prepared as shown in **Scheme 2a**. Starting from pentaerythritol, ε-CL was polymerized by ROP with $Sn(oct)_2$ as catalyst to give tetra-PCL-OH (**1**). The molar mass of **1** (10 kg mol^{-1}, ~2.5 kg mol^{-1} per arm) was adjusted by the molar ratio of pentaerythritol : ε-CL (1 : 87). As shown by NMR spectroscopy, [39, 43] the following esterification of the hydroxy terminal groups of **1** with compound **2** proceeded quantitatively. The NMR investigations also showed that **1** contained a small number of unreacted hydroxy groups on the pentaerythritol core (≤ 6 % three-arm stars).[43] During esterification with **2**, these hydroxy groups are also converted resulting in an average end group functionality of $f \geq 3.8$ (conversion $p \geq 95\%$) in tetra-PCL **3**.

The hydrophilic tetra-PEG-based **5** was synthesized using commercially available monodisperse tetra-PEG-OH with a molar mass of 10 kg mol^{-1}. After removal of low molecular weight fractions, the terminal hydroxy groups of tetra-PEG-OH were reacted first with mesyl chloride to give **4** and then with ammonia to yield amino-terminated tetra-PEG **5** (see **Scheme 2b**). Comparison of the ^{1}H NMR spectra of **1** and **3** as well as tetra-PEG-OH, **4** and **5** showed that the respective end group modification occurred quantitatively. The molar masses of **3** and **5** (see **Table 2**) were determined by ^{1}H NMR end group analysis (see SI **Figure S1** and **S2**) and SEC. There is a very good correlation between the number-average molar masses determined by NMR spectroscopy and SEC.

Due to the large amount of material required for the network syntheses, three batches with similar molar masses were synthesized for the hydrophobic (**3a-c**) as well as for the hydrophilic

component (**5a-c**). The deviations of the molar masses between the individual batches are small, indicating a very good reproducibility of the synthesis. In addition, all samples are characterized by narrow molar mass distributions, which is an essential prerequisite for the synthesis of model networks. Due to the very good agreement of the molecular parameters of the individual batches, in the following, no explicit reference to the respective batches used for further characterization and network synthesis will be made.

Table 2. Molecular characteristics of different batches of tetra-arm star polymers **3** and **5**

	3a	**3b**	**3c**	**5a**	**5b**	**5c**
$M_{n,NMR}$[a)] (kg mol^{-1})	11.1 ± 0.2	11.3 ± 0.2	10.5 ± 0.2	11.4 ± 0.2	10.8 ± 0.2	11.1 ± 0.2
$M_{n,SEC}$[b)] (kg mol^{-1})	11.4 ± 0.2	11.7 ± 0.1	11.0 ± 0.1	-	10.4 ± 0.3	11.0 ± 0.1
$M_{w,SEC}$[b)] (kg mol^{-1})	12.4 ± 0.2	12.6 ± 0.1	11.8 ± 0.0	-	10.6 ± 0.2	11.5 ± 0.3
Đ[b)]	1.09 ± 0.01	1.07 ± 0.1	1.07	-	1.02 ± 0.01	1.05 ± 0.01

[a)] based on ^{1}H NMR end group analysis (see SI **Figure S1** and **S2** and comments)

[b)] based on SEC (MALS/dRI detection) in THF (**3a-c**) and water (**5a-c**)

To assure the formation of homogeneous networks, a sufficiently high star polymer concentration in the reaction mixture and good polymer-solvent interactions are essential. Key parameters in this context are the Flory-Huggins interaction parameters χ between the polymers and the solvents and the overlap concentration c* of the star polymers in solution. The experimental data for χ in literature, see **Table 3**, are not really consistent and were measured mainly at temperatures around 100 °C outside of our temperature window for synthesis and analysis. If this is not the case like in Ref.[62] the data were computed from swelling measurements and thus, may contain a dependence on the model for elasticity and swelling.

Theoretical estimates for the interaction parameter can be made using the Hildebrand-Scott solubility parameter,[63] the Hansen method for the solubility parameters,[64, 65] or the Tian-Munk model,[66] whereby the latter is the most general approach, allowing also for negative interaction parameters as measured for chloroform. In the SI **Chapter 10**, we have compiled the original data regarding the corresponding solubility parameters and we provide a brief description how the interaction parameters were computed. The results of these computations are summarized in **Table 3**.

Table 3 Flory-Huggins interaction parameter χ of PEG and PCL in different solvents

χ [a)]	Toluene	THF	Chloroform	Reference
χ PEG	0.26 (100 °C)	0.30 (100 °C)	-0.55 (100 °C)	[67]
χ PEG [b)]	0.54 - 0.47 (85 - 105 °C)	-	-1.00 to -0.86 (85 - 105 °C)	[68]
χ PEG	-	0.38	-	[62]
χ_η PEG [c)]	0.38	0.41	-1.61	this work
χ_{HS} PEG [d)]	0.57	0.45	0.43	this work (SI)
$\chi_{\alpha=0.6}$ PEG [d)]	0.56	0.14	0.25	this work (SI)
χ_{TM} PEG [d)]	0.30	0.38	-1.04	this work (SI)
χ PCL	0.08 (100 °C)	0.13 (100 °C)	-0.40 to -0.22 (100 - 120 °C)	[67]
χ PCL	-0.01 - 0.07 (70 - 140 °C)	-	-	[69]
χ_η PCL [c)]	-0.05	0.07	-0.54	this work
χ_{HS} PCL [d)]	0.53	0.42	0.41	this work (SI)
$\chi_{\alpha=0.6}$ PCL [d)]	0.41	0.16	0.12	this work (SI)
χ_{TM} PCl [d)]	0.09	0.18	-0.71	this work (SI)

[a)] data refer to 25 °C if no explicit temperature is noted

[b)] for M_n = 10 kg mol^{-1}

[c)] based on viscosity data

[d)] computed in this work using the Hildebrand-Scott approach,[63, 67] (χ_{HS}), the Tian-Munk model,[66] (χ_{TM}), or the Hansen approach[64, 65] for $\alpha = 0.6$ ($\chi_{\alpha=6}$) as described in the SI.

When comparing with our viscosity data for dilute solutions of compounds **3** and **5** at different temperatures and in different solvents (see **Figure 2a**), only the Tian-Munk interaction parameter χ_{TM} (see **Table 3**) allows to put all measured overlap concentrations of a given polymer in the correct order. Moreover, χ_{TM} shows the best agreement with the published experimental data when assuming better solubility at elevated temperatures, as indicated by the viscosity data. Therefore, we use χ_{TM} as starting point to develop below an improved estimate χ_η that reproduces accurately the ratio of the measured intrinsic viscosities of both compounds, allowing for a quantitative comparison of data measured in different solvents.

As all solvents are good solvents according to χ_{TM}, we start with computing the square radius of gyration, R_g^2, of the star polymers in the particular good solvent

$$R_g^2 \approx b^2(1-2\chi_{TM})^{2\nu-1}\frac{1}{(2\nu+1)(2\nu+2)}\left(3-\frac{2}{f}\right)\left(\frac{N}{f}\right)^{2\nu} \quad (4)$$

This equation combines relations for the size of linear chains in good solvents[5, 70] with the dependence of R_g^2 on the number of star arms, f. Above, $\nu = 0.5876$ is the Flory exponent,[71] while the Kuhn length b and the number of Kuhn segments per star polymer, N, are given in the SI **Table S3**. In this table, we compiled literature data for geometric parameters of the polymer, from which b an N were computed.

Numerical results[72] for the ratio between the radius of gyration and the hydrodynamic radius, R_h, of self-avoiding walks are close to 1.58. A numerical test in the dilute regime using our simulation model for star polymers with a number of Kuhn segments comparable to the experiments provides 1.57. Experimental data lead to a ratio R_g/R_h that is typically smaller by 10-20 % as compared to these numerical data,[45] mainly due to the assumptions made for computing R_h. Therefore, we use

$R_g/R_h \approx 1.35 \pm 0.08$ to estimate R_h. These results are combined with the viscosity data to compute the ratio

$$z = \frac{M_w[\eta]}{N_A R_h R_g^2} \quad (5)$$

Here, N_A is Avogadro's constant. For linear chains, $z \approx 7$ is a constant in good solvent.[5] The corresponding z of star polymers is not known but can be expected to be larger, since the increased compactness of the molecules overcompensates the poorer draining of the solvent and the shift of the universal constant for viscosity with increasing f.[73, 74] We have computed z for all combinations between the polymers and the solvents of our study and obtain $z = 9.1 \pm 0.6$ when using χ_{TM}. Repeating this analysis with other estimates for the interaction parameter produces a significantly larger scatter for z supporting our observation that χ_{TM} fits best to the experimental data.

Assuming that z is a constant for a fixed $f = 4$ and not only for the linear case, $f = 2$, we invert the above computation starting from z = 9.1 and convert the viscosity data into experimentally based estimates for the interaction parameter, χ_η. These estimates are also listed in **Table 3** and have a high correlation with the experimental data for χ. The above procedure minimizes errors for individual interaction parameters, but cannot remove all errors on an absolute scale. The main benefit of the above approach is that χ_η is correct on a relative scale (within the error of the viscosity measurements) such that we can compare experimental data for different solvents with high accuracy.

A quantitative test of the above computations is possible with dynamic light scattering (DLS), since the hydrodynamic radius can be measured by this method. The DLS correlation functions of **3** and **5** in THF at 25 and 35 °C are depicted in **Figure 2b**. The data of **5** show two distinct

relaxation modes, indicating the formation of aggregates. This was accounted for by considering two independent decays for the data analysis, see the SI **Chapter 7** for a detailed description. The key result of this analysis is the hydrodynamic radius of both compounds (the data of **5** also contain an estimate for the cluster size) that is provided in the inset of **Figure 2b**. Using χ_η and the computation of R_g and R_h above provides $R_h = 2.8 \pm 0.2$ for compound **3** in perfect agreement with the DLS data. The same computation for compound **5** leads to a significantly smaller $R_h = 2.4 \pm 0.2$ reproducing the trend of the viscosity measurements, while the DLS data refer to an enlarged estimate for R_h. Apparently, the dynamics of individual stars interferes here with the dynamics of the clusters. However, the physical origin for the clustering is not clear and might be related to the differences in the oxygens between both polymers, which seems to be essential for the significant difference in the interaction parameter.

Altogether, the agreement for compound **3** strongly supports our analysis, suggesting that there are no large collective shifts to be expected on an absolute scale for our set of interaction parameters. Furthermore, a concentration of 70 g L^{-1} is sufficient for all three solvents to assure overlap of the star polymers. Therefore, this concentration is generally used as a benchmark for networks prepared at or above the overlap concentration c^*.

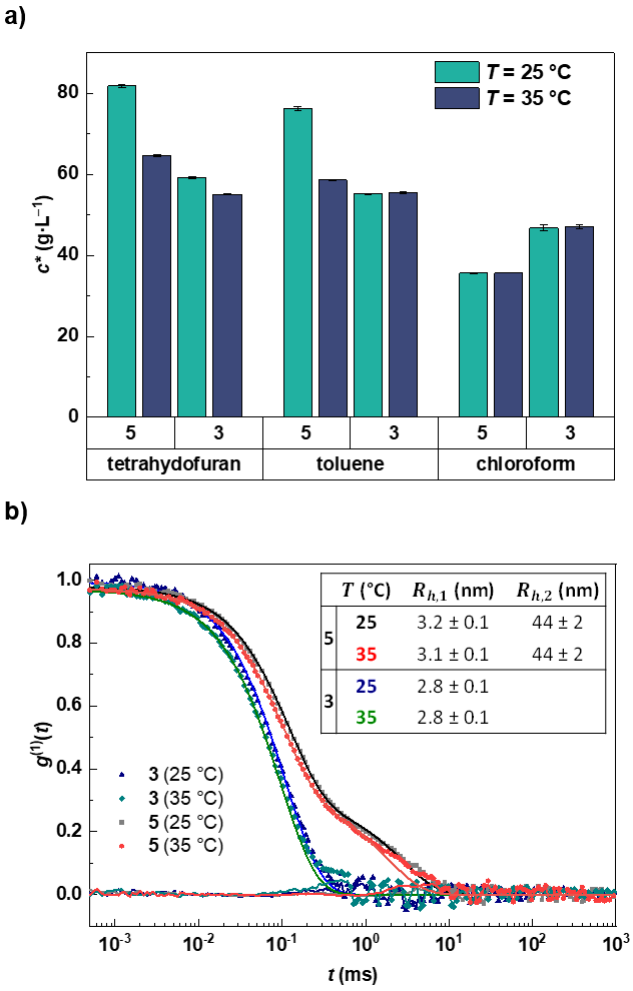

Figure 2. a) Overlap concentrations c* of star polymers **3** and **5** determined by viscometry in tetrahydrofuran, toluene, and chloroform at 25 and 35 °C. b) Hydrodynamic radii R_h and DLS autocorrelation functions (rectangles) with respective fit (solid lines) and corresponding residual fluctuations around zero for THF solutions (c = 30 g·L^{-1}) of PEG star polymer **5** at 25 (brown) and 35 °C (red) and PCL star polymer **3** at 25 (blue) and 35 °C (green) measured at a scattering angle of 30°. Corresponding fit parameters are summarized in the SI **Table S1**.

Synthesis, kinetics and gelation of amphiphilic co-networks $CN_{25,\,40,\,60}$

In order to investigate the gelation kinetics of the cross-linking reaction between **3** and **5** according to **Scheme 3**, time-dependent *in-situ* ^{1}H NMR measurements of the reacting mixtures were carried out at 25, 40, and 60 °C in THF-d_8 at a concentration of 70 g L^{-1}. In the following,

these networks will be referred to as **CN$_{25}$**, **CN$_{40}$** and **CN$_{60}$**. For each measurement, corresponding volume fractions of two stock solutions of the star polymers **3** and **5** were poured into an NMR tube and brought to the desired reaction temperature within ~5 min. The reaction was equimolar with respect to the reacting terminal groups. Selected spectra recorded during the reaction at 40 °C are shown in **Figure 3a**. For clarity, only the region of aromatic protons is shown. The intensities of the signals at 9.5 ppm ($H_{7'}$ of **CN**) and at 8.54 ppm (H_{10} of **3**) were used to calculate the conversion *p* of the cross-linking reaction (see also SI **Figure S3**). The signal assignment is based on the spectra of the corresponding star block copolymers, as described recently.[43] In **Figure 3a**, the $H_{7'}$ signal of the formed benzamide group appears already after 3 min, indicating that the reaction begins immediately after the solutions are poured together. However, the reaction is of intermediate rate and could be well followed up to conversion of *p* ~0.9 for **CN$_{40}$** and *p* ~ 0.8 for **CN$_{25}$** and **CN$_{60}$**. Continuing the reaction outside the spectrometer reveals that complete conversion could not be achieved under the given reaction conditions, even after a total reaction time of three days. The respective conversion-time curves for **CN$_{25,\ 40,\ 60}$** are shown in **Figure 3b.**

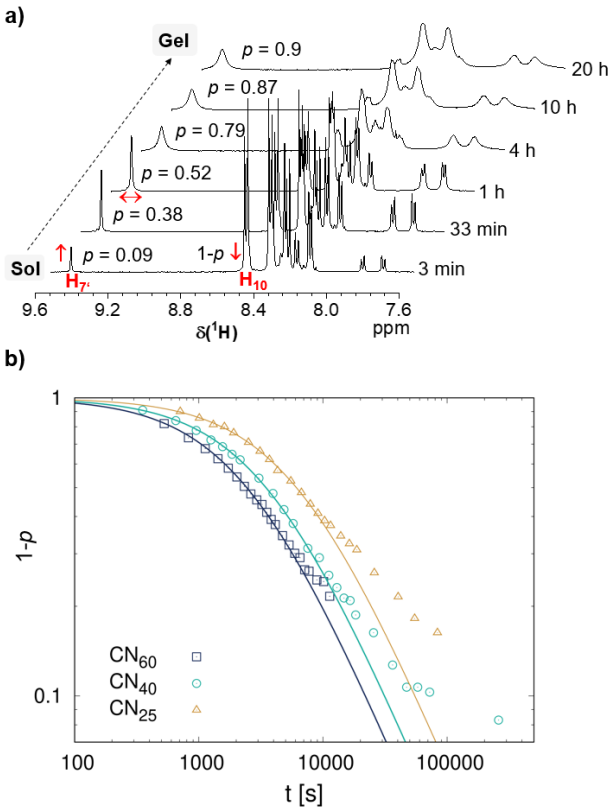

Figure 3. NMR spectroscopic monitoring of the cross-linking reaction between **3** and **5** in THF-d_8 at a concentration of 70 g L^{-1} (~ c*), a) Time-dependent ^{1}H NMR spectra (region of aromatic protons) recorded during the network formation of **CN_{40}** at 40 °C, b) (*1-p*)-time curves calculated from the signal intensities of $H_{7'}$ and H_{10} at three different temperatures (**$CN_{25,\,40,\,60}$**).

For a more detailed analysis of kinetics, we consider that the reactive groups are stoichiometrically balanced, $[3]_0 = [5]_0$. In this case, kinetics can be written as

$$\frac{d[3]}{dt} = -k[3][5] = -k[3]^2 \qquad (6)$$

with the solution

$$\frac{[3]}{[3]_0} = \frac{1}{1 + k[3]_0 t} = 1 - p. \qquad (7)$$

Here, t is the reaction time, k the reaction constant, and [3] and [5] are the concentrations of the two reactive groups of the star polymers **3** and **5** at time t. p is the conversion of the reactive groups and $[3]_0$ the initial concentration of the reactive groups.

A simple evaluation of an assumed second-order reaction with equimolar reactants **3** and **5** is possible with the plot of 1/[3] vs. t. The plots show a very good linear dependence up to conversions of ~60 % (see SI **Figure S5**) confirming that the reaction of the terminal groups of **3** and **5** follows over a wide range the kinetics of a second-order reaction (see **Table 4**). In a second approach, the data on the reaction kinetics were analyzed in two steps. First, the low time limit of the ratio of the concentrations $[3]/[3]_0$ of the reactive groups was fit to a modified form of equation (4) in the form of

$$\frac{[3]}{[3]_0} = 1 - p = \frac{1}{1 + k[3]_0(t + t_0)} \tag{8}$$

for the low t data with $p < 0.4$ in order to determine an effective time offset t_0. This offset accounts for sample handling and temperature equilibration in the NMR spectrometer in the initial period. For the three graphs in **Figure 3b**, we have shifted each data set along the time axis by the corresponding t_0 and plotted against equation (5). Up to $p \sim 0.6$, the reactions closely follow the predicted ideal reaction kinetics. Using the obtained k values at temperatures of 25, 40, and 60 °C from **Table 4**, the Arrhenius activation energy E_a of 21.8 ± 0.9 kJ mol^{-1} was determined. The corresponding ln k vs. 1/T plot and the associated calculation of E_a are shown in the SI in **Chapter 11** (**Figure S6**). A significant slowdown of kinetics is visible at higher conversions. This observation is equivalent to the behavior of the simulation data shown in the SI **Chapter 12**. Such a slowdown in a recombination reaction of two species at stoichiometric conditions is a signature of composition fluctuations.[75, 76] These become stationary after gelation as the star polymers are rapidly incorporated into the gel (see SI **Figure S7**). Therefore, the slowdown also is a measure

for the quality of the mixture. The onset of this process occurs at almost the same conversion as in the perfect mixtures of the simulations, indicating near perfect mixing conditions in the experiment. Regarding the NMR spectra in **Figure 3a**, it is noticeable that the signal widths widen significantly with increasing crosslinking. This is caused by the reduced mobility of the segments in the network.

For gel point determination, the time change of the line width at half height ($w_{1/2}$) of the signal $H_{7'}$ was determined and converted to the effective transverse relaxation time T_2^* (see **Figure 4**). The time axis was also corrected here by t_0. Gelation can be traced by a sudden drop in T_2^* from a nearly constant level prior to gelation.[77]

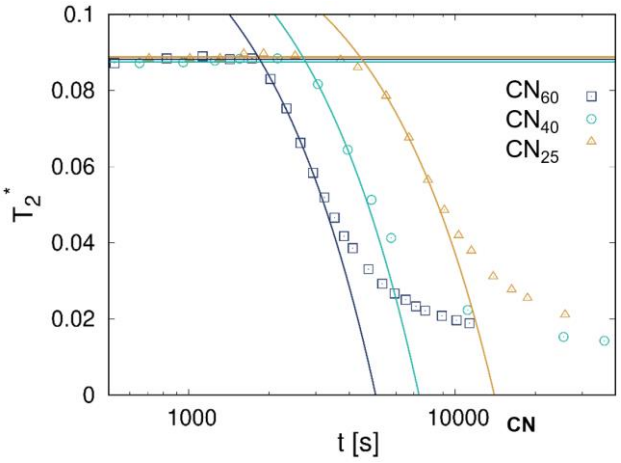

Figure 4 NMR gel point analysis of the sol-gel transition during the **CN** network formation. T_2^* relaxation time was determined from the linewidth at half height, $w_{1/2}$ (Hz), of signal $H_{7'}$ according $T_2^* = 1/(\pi w_{1/2})$.

Subsequently, the resulting gelation times t_c in **Table 4** were determined from the intersection of the horizontal lines with linear fits to the steepest descents of the data shown in **Figure 4** (note the logarithmic time axis). The gelation times refer to conversions at the gel point p_c according to

$$p_c = \frac{k[3]_0 t_c}{1 + k[3]_0 t_c} \tag{9}$$

The delay of the gel point conversion is, thus, computed from

$$\Delta p = p_c - p_{c,id} = \frac{k[3]_0 t_c}{1 + k[3]_0 t_c} - \frac{1}{f - 1} \tag{10}$$

where $p_{c,id}$ is the conversion at the ideal gel point for functionality $f = 4$. All results of this analysis are summarized in **Table 4**. For comparison, the gel point of the simulations at c* is located at a conversion of $p = 0.44 \pm 0.01$, which agrees within error with the experiments at all temperatures. This agreement shows that experiments and simulations were conducted at roughly the same overlap number of the star polymers, since the delay of the gel point is a universal function of the junction functionality and the overlap of the network strands.[60]

Table 4 Reaction kinetics and gel point determination by *in-situ* NMR spectroscopy

T (°C)	$[3]_0$, $[5]_0$ [a] (10^{-2} mol L^{-1})	k [b] (L mol^{-1} s^{-1})	t_c [c] (min)	p_c [d]	Δp [e]
25	1.22	0.013 (0.013)	73	0.42	0.09
40	1.22	0.024 (0.023)	46	0.44	0.11
60	1.22	0.034 (0.032)	31	0.43	0.10

[a] Concentration of the reactive groups, corresponds to an overall concentration of star polymers of 70 g L^{-1}

[b] reaction constant, values in brackets are based on the plot shown in the SI **Figure S5**

[c] gelation time

[d] conversion at gel point

[e] delay of the gel point conversion according to equation (10)

Characterization of amphiphilic co-networks

A series of ACNs were synthesized by equimolar conversion of star polymers **3** and **5** (see sample overview in **Table 1**). For the synthesis, corresponding aliquots of the stock solutions of **3** and **5** were poured together. Solvent, temperature, and polymer concentration were varied. After completion of the cross-linking reaction (~ 3 d), equilibrium volume swelling degrees Q_v of the co-networks were determined gravimetrically (see **Figure 5**). Swelling experiments were repeated 3 to 4 times for each sample (Q_{v1}, Q_{v2}…) where all swelling experiments were followed by a period of complete drying of the samples prior to the next swelling experiment.

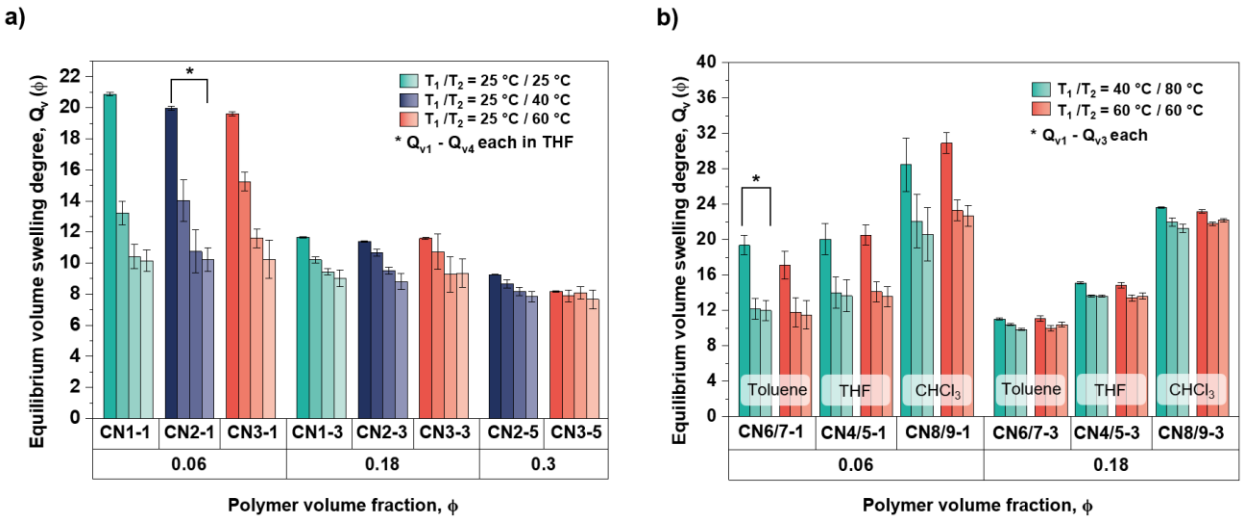

Figure 5. Equilibrium volume swelling degrees Q_v of ACNs synthesized under different reaction conditions (T, ϕ_0, solvent) and swollen with the same solvent. The columns for a given sample correspond to three to four consecutive swelling-drying cycles (Q_{v1} – Q_{v4}) from left to right, where the swelling starts from the preparation state. Different colors represent varying synthesis temperatures (T_1 = pre-gel point, T_2 = post-gel point). a) Co-networks synthesized in THF b) co-networks synthesized in toluene-d_8, THF-d_8, and $CDCl_3$, respectively.

Figure 5a shows equilibrium swelling degrees Q_v of samples synthesized in THF, while deuterated solvents (toluene-d_8, THF-d_8, $CDCl_3$) were used for the syntheses of the samples in

Figure 5b. The use of deuterated solvents enabled additional MQ-NMR studies on the gels obtained. However, we have to keep in mind that in some cases deuterated solvents may develop interactions significantly different from the protonated counterpart.[78] For the swelling experiments, the corresponding non-deuterated solvents were used. Both diagrams show that swelling from the preparation state (Q_{v1}) without intermediate drying delivers the highest swelling ratios. The reason for this is related to the slowdown of the reaction kinetics discussed in the preceding section: random diffusion of both compounds leads to a spontaneous formation and decay of local composition fluctuations during the concourse of the reactions. When most of the star polymers are attached to the gel, these composition fluctuations become static and turn into a distribution of local domains with varying stoichiometric imbalance. Kinetics in these domains vanish once reactive groups of the minority component are consumed, driving a continuous slowdown of the reaction.

Subsequent equilibrium swelling of the samples after cross-linking reduces the overlap between the molecules preventing complete reactions, drying causes the opposite effect: the overlap number of the star polymers grows[5] $\propto \phi^{1/(6\nu-2)}$, bringing previously separated end groups of star polymers in contact allowing for additional reactions. This effect is particularly pronounced for samples synthesized at low polymer concentration (ϕ_0 = 0.06), since the low ϕ_0 at preparation causes a slower kinetics and a lower maximum p, which is most increased by post-reaction due to a larger change in the overlap number upon drying compared to ϕ_0 = 0.18 and ϕ_0 = 0.30.

Apparently, the composition fluctuations of the co-networks of **Figure 5a** exceed the stochastic composition fluctuations of the perfectly mixed co-networks in the simulations, even though kinetics did not indicate a large discrepancy. This can be judged from the comparatively large sol fractions (see **Table 1**) in the experiments, see **Figure S7** in the SI for data around c^* and Ref.[27]

for simulation data at different concentrations (note the different definition of c^*). The reason for this difference is not clear at the moment and will be explored by additional computer simulations.

The swelling experiments also show that the synthesis temperature and thus, reaction kinetics has no significant influence on the network properties. Regarding the influence of the solvents (see **Figure 5b**), it is noticeable that synthesis and swelling in chloroform results in distinctly larger Q_v values. *A priori*, it is not clear whether this results from a different solvent quality or from differences in the network structure. However, this point can be clarified by plotting all Q_{v1} data and swelling data of the simulations in a universal plot where solvent quality and differences in N cancel out, see **Figure 6**.

This universal plot is obtained as follows. For the experimental data, we convert χ_η into an estimate for the excluded volume

$$\mathrm{v} = \left(1 - 2\chi_\eta\right)\mathrm{v}_s \tag{11}$$

where v_s is the unit volume of the Flory Huggins lattice that is set by the monomeric solvent molecules. In our co-networks, roughly half of the polymer is PEG and the other half PCL. Thus, we expect a sample average interaction parameter in a common non-selective solvent that is roughly the average of the corresponding χ_η estimates. This leads to a v/v_s of 0.67, 0.52, and 3.15 for toluene, THF, and chloroform, respectively. A cross-over between the semi-dilute good solvent regime and the concentrated regime is expected around $\phi^{**} \approx \mathrm{v}/\mathrm{v}_s$.[5] Since all networks were prepared and swell below ϕ^{**}, all experiments refer to swelling in the good solvent regime.

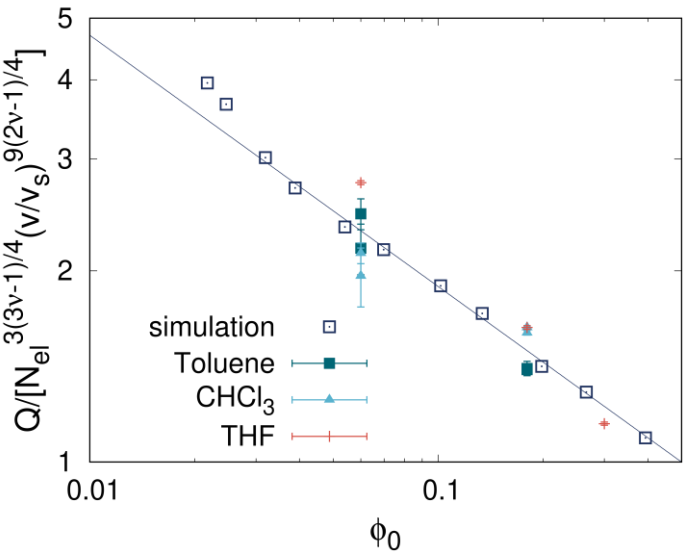

Figure 6. Equilibrium degree of swelling (first swelling) in the experiment and the simulations. The line is a power law fit to $\phi_0^{-0.40\pm0.01}$ to the simulation data for $\phi_0 > 0.03$. Multiple experimental data points at the same ϕ_0 refer to different temperature programs. The statistical error of the simulation data is comparable to the symbol size.

In the simulations, the excluded volume per monomer can be counted directly.[79] Exactly 8 lattice sites are blocked per monomer for the implicit solvent that fills the rest of the lattice leading to an excluded volume parameter for chain swelling of $8/b^3$ where $b \approx 2.73$ while at low concentrations, N refers to the number of independent segments of the self-avoiding walk. This provides $v/v_s \approx 0.39$ for the simulation data that all refer to swelling in the good solvent limit.

For swelling in the good solvent regime, scaling models[5, 80] predict for the entanglement free limit

$$Q \approx N^{3(3\upsilon-1)/4}\phi_0^{-1/4}(v/v_s)^{9(2\upsilon-1)/4} \qquad (12)$$

leading directly to the universal plot in **Figure 6**. Flory type mean field models[81, 82] arrive at nearly the same scaling as a function of N, but with a different scaling as a function of ϕ_0:

$$Q \propto N^{3/5}\phi_0^{-2/5}. \quad (13)$$

The data in **Figure 6** roughly collapse on a single line, supporting our analysis of the interaction parameters. Note that we have enforced a conversion of exactly $p = 0.95$ in the simulations that serves as a benchmark for the experimental systems. Accordingly, the experimental data are not far from conversions around $p \approx 0.95$. We further conclude that the large swelling in $CHCl_3$ results from the solvent quality and not from a lower conversion.

The exponent for ϕ_0 in **Figure 6** is in remarkable agreement with the mean field model prediction, however, this point has to be considered with care. It is expected that entanglements cause a stronger concentration dependence of the equilibrium degree of swelling as can be judged from swelling data on Olympic gels[83] $\propto \phi_0^{-0.72}$ and theoretical predictions up to $\propto \phi_0^{-1}$.[80] Network defects have a strong impact on the scaling of equilibrium swelling data.[81, 84] In particular, preparation of model networks at low ϕ_0 enhances the formation of network defects leading to a stronger dependence on ϕ_0. Such nonidealities are minimized by our network architecture. Exponents of 0.71 and 0.75 were reported[85] for model PDMS networks made of strands below the entanglement molecular weight or an exponent of 0.4 for gelatin gels.[86] For the data of Gnanou *et al.*[87] excluding the networks with a sol fraction beyond 10 %, see table 30 and 31 in Ref.[4], one obtains exponents of 0.52 and 0.92 for the short and the long polymers, respectively. A simulation study reported exponents increasing from 0.25 to 0.55 with increasing length of still quite short chains.[88] In contrast to this, we found only a very weak increase of the exponent for increasing N.[61] Altogether, the dependence on ϕ_0 has not been settled yet, but this open question could be advanced by using network architectures as ours that are less susceptible to network defects.

For the networks synthesized in THF (**CN1-1** to **CN3-5**), the degree of conversio p was determined by ^{1}H NMR end group analysis of spectra obtained by HR MAS NMR spectroscopy.

This technique provides well-resolved NMR spectra for swollen **CN** samples (see ESI **Figure S4**). For the measurements, the as-prepared gels were dried and re-swollen in $CDCl_3$ directly in the rotor insert. The state of the networks during these measurements is comparable to that during the second swelling experiment (Q_{v2}). It should be mentioned here that, for preparation-related reasons, measurement of the co-networks directly after synthesis has not yet been possible for the determination of conversion p. The calculation of p followed the procedure reported for the kinetics experiments and gave conversions $p \geq 0.98$ (see **Table 1**) for the investigated co-networks, with the exception of **CN2-5** (probably insufficient mixing before gelation). These measurements confirm that after removal of the sol fraction by Q_{v1} and subsequent evaporation of the synthesis solvent, virtually all benzoxazione groups were converted to benzamide groups.

Oscillatory shear rheology was used to investigate the viscoelastic behavior of the co-networks synthesized overnight at concentrations ranging from c* to 5c* in a mold at room temperature. The data of all measurements are summarized in the SI **Table S4**. **Figure 7** shows the typical rheological frequency sweep of a permanently cross-linked polymer gel with an elastic plateau of the storage modulus $G'(\omega)$ which dominates over the loss modulus $G''(\omega)$ for all concentrations. The loss modulus G" is more than two orders of magnitude smaller and develops a weak frequency dependence at low frequencies and concentrations, indicating minor contact problems. The onset of the relaxation of network defects is visible at larger concentrations and frequencies.

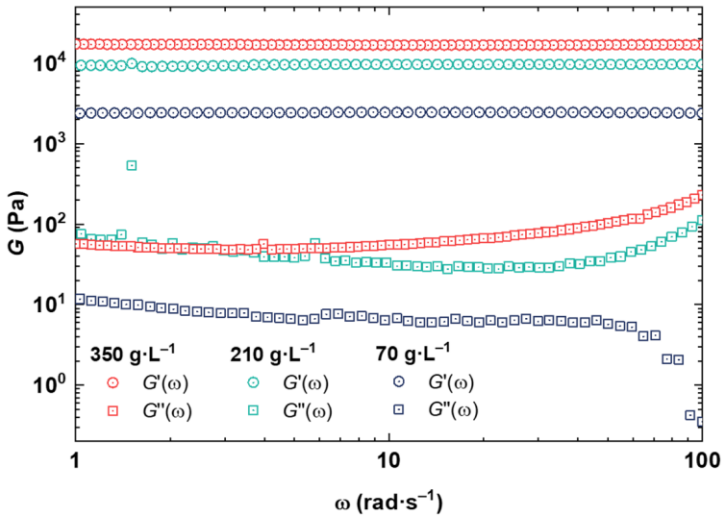

Figure 7. Oscillatory shear-rheology of amphiphilic polymer gels based on star polymers **3** and **5** gelated in a mold at c* (70 g L^{-1}, blue), 3c* (210 g L^{-1}, green) and 5c* (350 g L^{-1}, red) in toluene at preparation conditions.

For a quantitative test of our data we consider that PEG and PCL stars have molar masses of 10.7 and 11.8 kg mol^{-1}, respectively, and the average density of the polymers[47] in the dry networks is around 1.13 g mL^{-1}. Two stars of this type in a co-network produce four network strands, if all reactive groups are connected, leading to a molar mass around $M_{el} \approx 5.6$ kg mol^{-1} per network strand. The entanglement molar mass M_e in melts of PEG is around[67, 89] 2 kg mol^{-1} and does not exceed 3 kg mol^{-1} for PCL melts.[90, 91] The plateau modulus of entangled melts[92, 93] is $\propto \phi_0^{7/3}$ and there is $\phi_0 \leq 1/3$ for all of our samples. Thus, the about 2-3 entanglements per network strand in melts reduce to an entanglement contribution to modulus of the order of $kT/4$ per network strand for the largest ϕ_0, so that they become negligible for $\phi_0 \approx \phi^*$. Therefore, we use the phantom model prediction[5]

$$G_{ph} \approx \phi_0 \left(1 - \frac{2}{f}\right) \frac{\rho RT}{M_{el}} \qquad (14)$$

leading to $G_{ph}/\phi_0 \approx 252$ kPa for a quick quantitative test of the rheology data. A power law fit of the rheology data is in accord with $G_{ph} \approx {\phi_0}^{1.22\pm0.5} \times 64$ kPa, with an extrapolated amplitude at $\phi_0 = 1$ almost a factor of 4 below the expectations. The exponent for ϕ_0 is somewhat larger than unity similar to related work[94], indicating corrections due to entanglements for the largest ϕ_0 and a growing impact of a decreasing conversion and formation of finite loops[49, 95] towards small ϕ_0. Rheology during gelation indicates qualitatively that kinetics might be somewhat slower in toluene than in THF (a quantitative discussion of these results is omitted here due to the solvent evaporation observed in these measurements). Nevertheless, we expect a conversion of at least 0.8 for our samples when reacted overnight, which suffices to explain a drop in modulus only up to 40 %. Moreover, for our particular network architecture, the small loop corrections above the overlap threshold are too small to close the gap to the measurements. In a closely related work,[8] amphiphilic co-networks were synthesized using the same molecular architecture, similar molar masses of the star polymers, and a similar range of ϕ_0 with a quicker kinetics than in our study. Modulus in this study remains about a factor of 3 below the phantom estimate, which is not much different from our observations. The origin for this discrepancy is not understood at the moment.

One of the main concerns of this work was to find out how the reaction conditions affect the microstructure and homogeneity of the ACNs. Using the MQ experiment described in the experimental section, we analyzed samples synthesized under different conditions (**CN1-1** to **CN9-3**) in terms of their connectivities (see **Scheme 1**), isotropic (defect) fractions, and related average RDCs. We refrain from discussing the results of the sample series **CN1** to **CN3** in detail, which were dried after gelation and were subject to post-curing (see **Figure 5**). However, the connectivities of these samples are summarized in the SI (see **Table S5**).

First, we investigated differences between networks synthesized by our method (**PEG-2** and **CN5-3**) with networks synthesized according to Sakai *et al.*[26] (**PEG-1**). In addition to the different linkage mechanisms, it should be noted that the synthesis according to our method was carried out in the less polar solvent (toluene-d_8 versus D_2O). The polymer concentrations during the syntheses were comparable (~3c*, with neglectable small variations, see **Table 1**), but our oxazinone terminated tetra-stars are not compatible with water-based gel synthesis, precluding the corresponding control experiment.

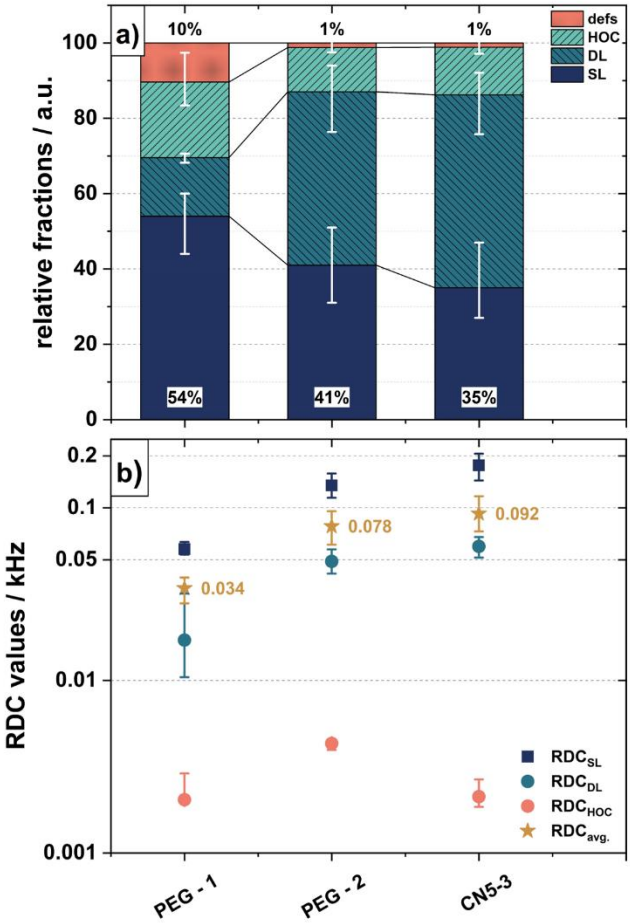

Figure 8. a) Comparison of different connectivity fractions obtained for different networks. **PEG-1** was synthesized in water according to Sakai *et al.*,[26] whereas **PEG-2** and **CN5-3** were synthesized in toluene according to our method. Note that the significant increase in the apparent

defect fraction for the Sakai network arises mainly from HDO, which can be formed by interaction of D_2O with moisture, b) corresponding RDC values and the fraction-weighted average RDC of the presented samples and connectivity fractions.

In **Figure** 8, it can be seen that the SL fraction of the gels synthesized by our method (**PEG-2** and also **CN5-3**) is significantly lower (13-19 %) than for of the gel synthesized according to Sakai (**PEG-1**). This in fact applies to all co-networks mentioned in this work (see SI **Table S5**). In comparison to earlier studies on Sakai's tetra-PEG networks, this deviation is even more pronounced.[33] There, the SL fraction (> 60 %) is close to the value expected for a randomly linked network. The dominance of the double links over the single links in our networks is surprising. Possible reasons for this are discussed below. Interestingly, we also find considerably larger RDC values in our gels, which cannot be explained yet. It is assumed that the deviations may arise from the different linking chemistry or from the overall PEG star conformation in the different polar solvents used for the syntheses.

For further investigation on factors influencing the microstructure of our amphiphilic PEG-PCL co-networks, sample series with different parameter variations (see **Table 1**) were synthesized for checking the influence of (i) network composition (PEG-PCL co-network vs. PEG-PEG network with benzoxazinone/amino end groups), (ii) solvent and (iii) temperature programs during synthesis. Aspect (i) is also addressed in **Figure 8**, whereas **Figure 9** shows the rest of the results.

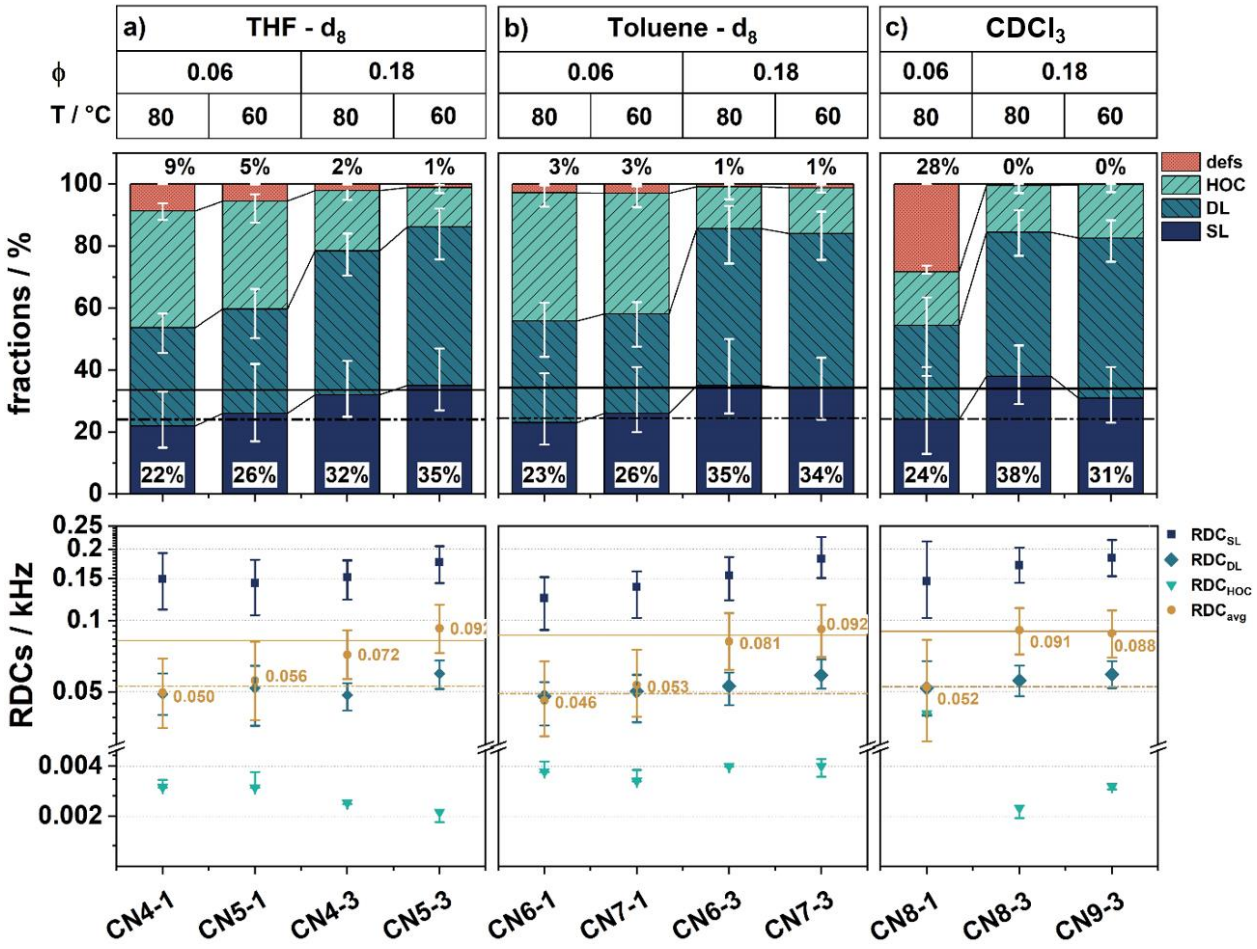

Figure 9. Connectivities and RCSs values of ACNs synthesized in a) THF-d_8, b) toluene-d_8, and c) $CDCl_3$. The syntheses were carried out at two different concentrations (ϕ = 0.06, 0.18) and two different temperature programs were applied (pre- and post-gel temperature = 60/60 °C and 40/80 °C, respectively). The reaction conditions are indicated above the diagrams. Only the highest reaction temperature is given (60, 80 °C).

(i): The most fundamental difference between our networks and a PEG-PEG gel is the fact that we have stars made of different polymers. The interaction parameters in **Table 3** show that no miscibility problems should arise related to the polymers. Moreover, for **PEG-2**, synthesized by the oxazinone coupling reaction referred to above, the same qualitative trend of a decreased SL fraction (in comparison to the data by Lange *et al.*[33]) was found (see **Figure 8**), ruling out the

polymers as source of this discrepancy. Still, we find a slight quantitative increase in the estimated fraction of single links from 35 % to 41 % on going from ACN to homo-PEG gel, although the actual polymer fraction upon synthesis was even slightly lower for the latter. We want to remind here that although this trend is within the shown error bars, the error bars are to be seen as systematic deviations arising from a slight unambiguity in the used fit function, meaning that if the upper boundary is chosen for the PEG-PCL network, it also has to be chosen for the PEG-PEG network (see Experimental Section and **Figure 1**).

(ii): To investigate the solvent influence on the connectivities, three solvents with different polarity were used in the synthesis (THF-d_8, toluene-d_8, $CDCl_3$). Unexpectedly, no significant difference between all three solvents, neither in the overall connectivity distribution nor in the RDC values were found (see **Figure 9**). Regardless of the choice of solvent, the SL fraction is well below the expectations. This indicates that the biased connectivity distribution cannot be attributed to different polarities of the solvents, and therefore not to slightly different hydrodynamic radii R_h or overlap concentrations c* of the tetra-stars.

(iii): The last possibly relevant structure-determining parameter is the reaction temperature. From the theoretical point of view, it was expected that at lower reaction temperatures and so at lower reaction rates the forming network would be able to relax better, resulting in higher homogeneity. However, at low temperatures, differences in the affinity of the two tetra-stars to the solvents used may become more pronounced resulting in a larger difference in the respective c* values. This may have a negative impact on the network structure. To gain a better insight on the temperature effect on the connectivity distribution, the temperature before and after the gel point was varied. Two different temperature protocols were applied (40 °C pre- and 80 °C post-gel

temperature vs. 60 °C during the whole synthesis). Again, the results (see **Figure 9**) show that the temperature has a negligible effect on the connectivity distribution.

A noticeable influence on the connectivity distribution seems to be exerted by the concentration of the stars. In the networks synthesized at higher concentrations (~3c*, ϕ_0 = 0.18), the SL fraction tends to be higher, while the HOC fraction and the fraction of defects (defs) appears to be distinctly lower. This trend is even more evident in sample **CN3-5** (see SI, **Table x**), which was synthesized at ~5c* but at a slightly different temperature program (25 °C pre- and 60 °C post-gel temperature). For this network, the highest SL fraction (~52 %) was found, which is very close to the value of the **PEG-1** network synthesized according to Sakai *et al.*[26] (54 %, see **Figure 8**). For this sample the lowest Q_v value was found (see **Figure 7a**).

Overall, the MQ studies show that for our networks the influence of the reaction conditions on the microstructure is small. Apart from the obvious influence of concentration (the higher above c*, the more single links), the reaction solvents and temperature do not affect the microstructure significantly. Rather, it can be concluded that the synthesis presented here is already in an optimized state, covering a variety of different conditions with reliable and reproducible outcome. Yet, the reason for the differences compared to the water-based hydrogels from Sakai *et al.*[26] is still unclear.

A non-trivial aspect to consider could be specific interactions of the end groups of the tetra-stars used by us. In contrast to the Sakai gels, one tetra-star possesses aromatic oxazinone terminal groups, which are assumed to interact with each other or with the linking groups formed during the synthesis by favorable van-der-Waals or π–π interactions. The polar nitro substituent on the oxazinone group could further enhance specific interactions. The resulting increase in local concentration of oxazinone groups could promote a formation of double links.

Still, it should be stressed that all data sets can be well fitted with the assumed 3-component model for the polymer connectivities, which, despite the somewhat biased connectivity fractions, indicates that the overall network has a model-like network structure with the expected well-defined crosslink distribution. Alternative modelling procedures that include distributions for RDC values and fractions of connectivities do not provide an equally good fit, as can be seen already by the prominent peak in the 7 - 15 ms regime of the I_{DQ} curves.

CONCLUSIONS

The method presented here for the preparation of ACNs by hetero-complementary linkage of oxazinone- and amino-terminated tetra-arm stars has proved to be extremely robust with respect to the synthesis conditions applied. Regardless of widely varying reaction parameters (T, ϕ, solvent), networks obtained differed only slightly with respect to their properties.

Kinetic studies of the crosslinking reaction performed by *in situ* NMR measurements allowed the reaction to be followed in time and confirm a second order reaction up to conversions of about 60 %. Based on the changing signal widths of certain NMR signals, gel point could be determined.

The overlap concentrations of both tetra-arm stars in THF, toluene, and $CHCl_3$ were determined by viscometry. We have computed estimates for the interaction parameters using the Hildebrand-Scott approach,[63] the Hansen approach,[64, 65] and the model of Tian and Munk. [66] The latter provides the best agreement with the viscometry data. We have combined our viscosity measurements with the Tian Munk estimate to obtain an improved estimate that correctly considers relative differences between the solvents used. These improved estimates seem to be reasonable approximations of the interaction parameters, since we can collapse all experimental and simulation data on equilibrium swelling in a universal plot. Furthermore, quantitative agreement was obtained between the

hydrodynamic radii determined by DLS in different solvents when the interaction parameters determined according to our estimation were applied.

Rheological characterization of the as-prepared gels leads to the same qualitative trends as reported for other hetero-complementary coupled networks of star polymers.[8] Modulus data on a quantitative basis are clearly below the expectations and in the range of recent experiments on comparable co-polymer gels.[8]

The equilibrium swelling degrees show a power law dependence on the polymer volume fraction at preparation, $\phi_0^{-0.40\pm0.01}$. This dependence is in between the scaling limits of entanglement-free networks and entanglement dominated systems and is only coincidentally close to the classical prediction.[61]

An essential aspect of the work was to find out which influence the reaction conditions have on the network microstructure. For this purpose, MQ NMR investigations were carried out which provided information on occurring connectivities (see **Scheme 1**) and possible network defects. We observe significant differences to previously studied tetra-PEG networks regarding the frequency of double links. These differences cannot be explained by different interactions between polymers and solvents but could be related to specific interaction of the linking groups in the network. To verify this, additional investigations are intended which include alternative linking reactions for which such interactions are varied systematically.

ASSOCIATED CONTENT

Supporting Information. The Supporting Information is available free of charge. Additional figures including the characterization and analysis methods of star polymer **3** and **5** as well as of the ACNs are presented.

AUTHOR INFORMATION

Corresponding Authors

Dr. Frank Böhme, Leibniz-Institut für Polymerforschung Dresden e. V, Hohe Straße 6, 01069 Dresden, Germany, Email: boehme@ipfdd.de

Prof. Kay Saalwächter, Institut für Physik- NMR, Martin-Luther-Universität Halle-Wittenberg, Betty-Heimann-Str. 7, 06120 Halle, Germany Email: kay.saalwaechter@physik.uni-halle.de

Dr. Michael Lang, Leibniz-Institut für Polymerforschung Dresden e. V, Hohe Straße 6, 01069 Email: lang@ipfdd.de

Author Contributions

All authors have given approval to the final version of the manuscript.

ACKNOWLEDGMENT

This work was carried out as part of the research collaboration "Adaptive Polymer Gels with Model Network Structure" (FOR2811), funded by the German Research Foundation (DFG), grant 397384169, and the individual grants 423514254, 423478088, 423435302, 423373052. The authors thank Prof. Albena Lederer for the opportunity to perform macromolecular structure

analysis using size exclusion chromatography, and Alissa Seifert and Christina Harnisch for performing these measurements.

REFERENCES

(1) Rikkou-Kalourkoti, M.; Patrickios, C. S.; Georgiou, T. K., Model Networks and Functional Conetworks. In *Polymer Science: A Comprehensive Reference*, Matyjaszewski, K.; Möller, M., Eds. Elsevier: Amsterdam, **2012**, 293-308.

(2) Patrickios, C. S.; Georgiou, T. K. *Curr. Opin. Colloid Interface Sci* **2003,** 8, (1), 76-85.

(3) Hernández-Ortiz, J. C.; Vivaldo-Lima, E. *Handbook of polymer synthesis, characterization, and processing* **2013**, 187-204.

(4) Hild, G. *Prog. Polym. Sci.* **1998,** 23, (6), 1019-1149.

(5) Rubinstein, M.; Colby, R. H., *Polymer physics*. Oxford university press, New York, **2003**.

(6) Erdodi, G.; Kennedy, J. P. *Prog. Polym. Sci* **2006,** 31, (1), 1-18.

(7) Yamamoto, K.; Ito, E.; Mori, Y. *Macromol. Symp.* **2019,** 385, (1), 1800181.

(8) Apostolides, D. E.; Patrickios, C. S.; Sakai, T.; Guerre, M.; Lopez, G.; Ameduri, B.; Ladmiral, V.; Simon, M.; Gradzielski, M.; Clemens, D.; Krumm, C.; Tiller, J. C.; Ernould, B.; Gohy, J. F. *Macromolecules* **2018,** 51, (7), 2476-2488.

(9) Hiroi, T.; Kondo, S.; Sakai, T.; Gilbert, E. P.; Han, Y. S.; Kim, T. H.; Shibayama, M. *Macromolecules* **2016,** 49, (13), 4940-4947.

(10) Künzler, J.; Ozark, R. *J. Appl. Polym. Sci.* **1997,** 65, (6), 1081-1089.

(11) Nicolson, P. C.; Vogt, J. *Biomaterials* **2001,** 22, (24), 3273-3283.

(12) Friends, G. D.; Kunzler, J. F.; Ozark, R. M. *Macromol. Symp.*, **1995**, 98, (1), 619-631.

(13) Iván, B.; Kennedy, J. P.; Mackey, P. W., Amphiphilic Networks. In *Polymeric Drugs and Drug Delivery Systems*, ACS, **1991**, Vol. 469, 203-212.

(14) Kennedy, J. P.; Fenyvesi, G.; Levy, R. P.; Rosenthal, K. S. *Macromol. Symp.* **2001,** 172, 57-66.

(15) Kennedy, J. P.; Rosenthal, K. S.; Kashibhatla, B. *Des. Monomers Polym.* **2004,** 7, (6), 485-494.

(16) Lin, C.; Gitsov, I. *Macromolecules* **2010,** 43, (23), 10017-10030.

(17) Schöller, K.; Küpfer, S.; Baumann, L.; Hoyer, P. M.; De Courten, D.; Rossi, R. M.; Vetushka, A.; Wolf, M.; Bruns, N.; Scherer, L. J. *Adv. Funct. Mater.* **2014,** 24, (33), 5194-5201.

(18) Grossen, P.; Witzigmann, D.; Sieber, S.; Huwyler, J. *J. Control Release* **2017,** 260, 46-60.

(19) Ozcelik, B.; Brown, K. D.; Blencowe, A.; Ladewig, K.; Stevens, G. W.; Scheerlinck, J.-P. Y.; Abberton, K.; Daniell, M.; Qiao, G. G. *Adv. Healthc. Mater.* **2014,** 3, (9), 1496-1507.

(20) Guzman, G.; Nugay, T.; Nugay, I.; Nugay, N.; Kennedy, J.; Cakmak, M. *Macromolecules* **2015,** 48, (17), 6251-6262.

(21) Sittko, I.; Kremser, K.; Roth, M.; Kuehne, S.; Stuhr, S.; Tiller, J. C. *Polymer* **2015,** 64, 122-129.

(22) Huang, C.-S.; Jakubowski, K.; Ulrich, S.; Yakunin, S.; Clerc, M.; Toncelli, C.; Rossi, R. M.; Kovalenko, M. V.; Boesel, L. F. *Nano Energy* **2020,** 76, 105039.

(23) Ulrich, S.; Osypova, A.; Panzarasa, G.; Rossi, R. M.; Bruns, N.; Boesel, L. F. *Macromol. Rapid Commun.* **2019,** 40, (21), 1900360.

(24) Apostolides, D. E.; Patrickios, C. S.; Sakai, T.; Guerre, M.; Lopez, G.; Améduri, B.; Ladmiral, V.; Simon, M.; Gradzielski, M.; Clemens, D.; Krumm, C.; Tiller, J. C.; Ernould, B.; Gohy, J.-F. *Macromolecules* **2018,** 51, (7), 2476-2488.

(25) Lang, M. *Macromol. Symp.* **2019,** 385, (1), 1800168.

(26) Sakai, T.; Matsunaga, T.; Yamamoto, Y.; Ito, C.; Yoshida, R.; Suzuki, S.; Sasaki, N.; Shibayama, M.; Chung, U. I. *Macromolecules* **2008,** 41, (14), 5379-5384.

(27) Lang, M.; Schwenke, K.; Sommer, J. U. *Macromolecules* **2012,** 45, (11), 4886-4895.

(28) Lang, M. *ACS Macro Lett.* **2018,** 7, (5), 536-539.

(29) Matsunaga, T.; Sakai, T.; Akagi, Y.; Chung, U.-i.; Shibayama, M. *Macromolecules* **2009,** 42, (4), 1344-1351.

(30) Matsunaga, T.; Sakai, T.; Akagi, Y.; Chung, U.-i.; Shibayama, M. *Macromolecules* **2009,** 42, (16), 6245-6252.

(31) Hiroi, T.; Ohl, M.; Sakai, T.; Shibayama, M. *Macromolecules* **2014,** 47, (2), 763-770.

(32) Schwenke, K.; Lang, M.; Sommer, J. U. *Macromolecules* **2011,** 44, (23), 9464-9472.

(33) Lange, F.; Schwenke, K.; Kurakazu, M.; Akagi, Y.; Chung, U. I.; Lang, M.; Sommer, J. U.; Sakai, T.; Saalwachter, K. *Macromolecules* **2011,** 44, (24), 9666-9674.

(34) Kamata, H.; Akagi, Y.; Kayasuga-Kariya, Y.; Chung, U.; Sakai, T. *Science* **2014,** 343, (6173), 873-875.

(35) Nakagawa, S.; Li, X.; Kamata, H.; Sakai, T.; Gilbert, E. P.; Shibayama, M. *Macromolecules* **2017,** 50, (8), 3388-3395.

(36) Truong, V.; Blakey, I.; Whittaker, A. K. *Biomacromolecules* **2012,** 13, (12), 4012-4021.

(37) Jakisch, L.; Komber, H.; Böhme, F. *Macromol. Mater. Eng.* **2007,** 292, (5), 557-570.

(38) Zhang, H.; Jakisch, L.; Komber, H.; Voit, B.; Böhme, F. *Tetrahedron* **2013,** 69, (18), 3656-3663.

(39) Jakisch, L.; Garaleh, M.; Schäfer, M.; Mordvinkin, A.; Saalwächter, K.; Böhme, F. *Macromol. Chem. Phys.* **2018,** 219, (3), 1700327.

(40) Wang, H. Y.; Qin, A. W.; Li, X.; Zhao, X. Z.; Liu, D. P.; He, C. J. *J. Polym. Sci. Pol. Chem.* **2015,** 53, (21), 2537-2545.

(41) Zare, Y.; Dabbaghi, A.; Rahmani, S. *Polym. Adv. Technol.* **2019,** 1-12.

(42) Yuan, Y.; Zhang, A.-K.; Ling, J.; Yin, L.-H.; Chen, Y.; Fu, G.-D. *Soft Matter* **2013,** 9, (27), 6309-6318.

(43) C. Bunk, H. Komber, N. Fribiczer, M. Geisler, L. Jakisch, S. Seiffert, F. Böhme. *submitted* **2022**.

(44) Ishii, S.; Kokubo, H.; Hashimoto, K.; Imaizumi, S.; Watanabe, M. *Macromolecules* **2017,** 50, (7), 2906-2915.

(45) Burchard, W., Solution properties of branched macromolecules. In *Branched polymers II*, Springer: **1999**, 113-194.

(46) Schulz, v. G.; Blaschke, F. *J. prakt. Chem.* **1941,** 158, (1-8), 130-135.

(47) http://polymerdatabase.com/polymer%20physics/Polymer%20Density.html

(48) Lang, M. *Macromolecules* **2013,** 46, (24), 9782-9797.

(49) Lang, M. *Macromolecules* **2019,** 52, (16), 6266-6273.

(50) Ahmadi, M.; Löser, L.; Fischer, K.; Saalwächter, K.; Seiffert, S. *Macromol. Chem. Phys.* **2020,** 221, (1), 1900400.

(51) Nicolella, P.; Koziol, M. F.; Löser, L.; Saalwächter, K.; Ahmadi, M.; Seiffert, S. *Soft Matter* **2022**.

(52) Chassé, W.; Valentín, J. L.; Genesky, G. D.; Cohen, C.; Saalwächter, K. *J. Chem. Phys.* **2011,** 134, (4), 044907.

(53) Hohwy, M.; Jakobsen, H. J.; Eden, M.; Levitt, M. H.; Nielsen, N. C. *J. Chem. Phys.* **1998,** 108, (7), 2686-2694.

(54) Müller, T.; Wengenmayr, M.; Dockhorn, R.; Knespel, M., LeMonADE-project/LeMonADE-GPU: Release v1.2. Zenodo: **2021**.

(55) Wengenmayr, M.; Dockhorn, R.; Mller, T.; Rabbel, H.; Jentzsch, C.; Werner, M. **2020**.

(56) Carmesin, I.; Kremer, K. *Macromolecules* **1988,** 21, (9), 2819-2823.

(57) Wittmer, J.; Beckrich, P.; Meyer, H.; Cavallo, A.; Johner, A.; Baschnagel, *Phys. Rev. E.* **2007,** 76, (1), 011803.

(58) Gerstl, C.; Schneider, G. J.; Pyckhout-Hintzen, W.; Allgaier, J. r.; Willbold, S.; Hofmann, D.; Disko, U.; Frielinghaus, H.; Richter, D. *Macromolecules* **2011,** 44, (15), 6077-6084.

(59) Lee, H.; Venable, R. M.; MacKerell Jr, A. D.; Pastor, R. W. *Biophys. J.* **2008,** 95, (4), 1590-1599.

(60) Lang, M.; Müller, T. *Macromolecules* **2020,** 53, (2), 498-512.

(61) M. Lang, R. S., L. Löser, C. Bunk, N. Fribiczer, S. Seiffert, F. Böhme, K. Saalwächter. *submitted* **2022**.

(62) Rebello, N. J.; Beech, H. K.; Olsen, B. D. *ACS Macro Lett.* **2021,** 10, (5), 531-537.

(63) Hildebrand, J. H.; Scott, R. L. *The solubility of nonelectrolytes*; Dover Publications: **1964**.

(64) Hansen, C. M. *Hansen solubility parameters*; CRC Press: Florida **2007;** 2.

(65) Hansen, C. M. *Danish Technical: Copenhagen* **1967;** 14.

(66) Tian, M.; Munk, P. *J. Solut. Chem.* **1995,** 24, (3), 267-284.

(67) Mark, J. E., *Physical properties of polymers handbook*. Springer: **2007**; Vol. 1076.

(68) Adamska, K.; Voelkel, A. *J. Chromatogr. A* **2006,** 1132, (1-2), 260-267.

(69) Sarac, A.; Şakar, D.; Cankurtaran, O.; Karaman, F. Y. *Polym. Bull.* **2005,** 53, (5), 349-357.

(70) Hammouda, B., SANS from homogeneous polymer mixtures: A unified overview. In *Polymer Characteristics*, Springer: **1993**; 87-133.

(71) Clisby, N. *Phys. Rev. Lett.* **2010,** 104, (5), 055702.

(72) Clisby, N.; Dünweg, B. *Phys. Rev. E* **2016,** 94, (5), 052102.

(73) Weissmüller, M.; Burchard, W. *Acta Polym.* **1997,** 48, (12), 571-578.

(74) Shida, K.; Ohno, K.; Kimura, M.; Kawazoe, Y.; Nakamura, Y. *Macromolecules* **1998,** 31, (7), 2343-2348.

(75) Ovchinnikov, A.; Zeldovich, Y. B. *Chem. Phys.* **1978,** 28, (1-2), 215-218.

(76) Kang, K.; Redner, S. *Phys. Rev. Lett.* **1984,** 52, (12), 955.

(77) Saalwächter, K.; Gottlieb, M.; Liu, R.; Oppermann, W. *Macromolecules* **2007,** 40, (5), 1555-1561.

(78) Yuan, G.; Hammouda, B. *Polymer* **2019,** 166, 178-183.

(79) Lang, M.; Rubinstein, M.; Sommer, J.-U. *ACS Macro Lett.* **2015,** 4, (2), 177-181.

(80) Obukhov, S. P.; Rubinstein, M.; Colby, R. H. *Macromolecules* **1994,** 27, (12), 3191-3198.

(81) Bastide, J.; Picot, C.; Candau, S. *J. Macromol. Sci. Phys.* **1981,** 19, (1), 13-34.

(82) Flory, P. J., *Principles of polymer chemistry*. Cornell university press: **1953**.

(83) Lang, M.; Fischer, J.; Werner, M.; Sommer, J.-U. *Phys. Rev. Lett.* **2014,** 112, (23), 238001.

(84) Lang, M.; John, A.; Sommer, J.-U. *Polymer* **2016,** 82, 138-155.

(85) Candau, S.; Peters, A.; Herz, J. *Polymer* **1981,** 22, (11), 1504-1510.

(86) Klepko, V.; Mel'nichenko, Y. B. *Polymer* **1995,** 36, (26), 5057-5059.

(87) Gnanou, Y.; Hild, G.; Rempp, P. *Macromolecules* **1987,** 20, (7), 1662-1671.

(88) Chen, Z.; Cohen, C.; Escobedo, F. A. *Macromolecules* **2002,** 35, (8), 3296-3305.

(89) Niedzwiedz, K.; Wischnewski, A.; Pyckhout-Hintzen, W.; Allgaier, J.; Richter, D.; Faraone, A. *Macromolecules* **2008,** 41, (13), 4866-4872.

(90) Gimenez, J.; Cassagnau, P.; Michel, A. *J. Rheol.* **2000,** 44, (3), 527-547.

(91) Sangroniz, L.; Barbieri, F.; Cavallo, D.; Santamaria, A.; Alamo, R.; Müller, A. *Eur. Polym. J.* **2018,** 99, 495-503.

(92) Adam, M.; Delsanti, M. *J. Phys.* **1983,** 44, (10), 1185-1193.

(93) Colby, R. H.; Fetters, L. J.; Funk, W. G.; Graessley, W. W. *Macromolecules* **1991,** 24, (13), 3873-3882.

(94) Akagi, Y.; Matsunaga, T.; Shibayama, M.; Chung, U.-i.; Sakai, T. *Macromolecules* **2010,** 43, (1), 488-493.

(95) Zhong, M.; Wang, R.; Kawamoto, K.; Olsen, B. D.; Johnson, J. A. *Science* **2016,** 353, (6305), 1264-1268.